

Detection of δ Scuti pulsators in the eclipsing binaries observed by TESS

XINGHAO CHEN,^{1,2} XU DING,^{1,2} LIANTAO CHENG,³ XIAOBIN ZHANG,⁴ YAN LI,^{1,5,6,7} KAIFAN JI,¹ JIANPING XIONG,^{4,6}
 XUZHI LI,^{8,9} AND CHANGQING LUO⁴

¹Yunnan Observatories, Chinese Academy of Sciences, P.O. Box 110, Kunming 650216, China

²Key Laboratory for Structure and Evolution of Celestial Objects, Chinese Academy of Sciences, P.O. Box 110, Kunming 650216, China

³School of Opto-electronic Engineering, Zaozhuang University, Zaozhuang 277160, China

⁴Key Laboratory of Optical Astronomy, National Astronomical Observatories, Chinese Academy of Sciences, Beijing, 100012, China

⁵Key Laboratory for Structure and Evolution of Celestial Objects, Chinese Academy of Sciences, P.O. Box 110, Kunming 650216, China

⁶University of Chinese Academy of Sciences, Beijing 100049, China

⁷Center for Astronomical Mega-Science, Chinese Academy of Sciences, 20A Datun Road, Chaoyang District, Beijing, 100012, China

⁸Deep Space Exploration Laboratory, Department of Astronomy, University of Science and Technology of China, Hefei, 230026, China

⁹School of Astronomy and Space Sciences, University of Science and Technology of China, Hefei, 230026, China

ABSTRACT

Based on 2-minute cadence TESS data from sectors 1-50, we report the results of the systematic extraction of δ Scuti-type pulsations in the 6431 eclipsing binaries with orbital periods shorter than 13 days. A total number of 242 pulsators were found in those systems, including 143 new discoveries. We examined their pulsation properties based on the H-R diagram and the relationships between the dominant pulsation period P_{dom} , orbital period P_{orb} , and effective temperature T_{eff} . As a consequence, 216 targets are likely δ Scuti stars (123 new), 11 likely γ Doradus- δ Scuti hybrid stars (8 new), 5 likely β Cephei stars (4 new), 4 likely δ Scuti- γ Doradus hybrid stars (3 new), 3 likely Maia stars (3 new), 2 likely pulsating red giants (1 new), and a new unclassified star. As for the 6 new δ Scuti pulsators in eclipsing binaries with $P_{\text{orb}} < 0.65$ days, we found that 3 of them significantly exceed the upper limits of the $P_{\text{dom}}/P_{\text{orb}}$ ratio. This may indicate that P_{dom} and P_{orb} are uncorrelated for them. Finally, we statistically analyzed the dominant pulsation periods of the 216 δ Scuti stars in eclipsing binaries. Those stars concentrate around 225 μ Hz and the proportion of stars in the high-frequency region is significantly higher than that of single stars, which could be ascribed to the mass transfer process.

Keywords: Eclipsing binary stars; Stellar oscillations; Pulsating variable stars; Delta Scuti variable stars

1. INTRODUCTION

Eclipsing binaries with pulsating components are very attractive objects and also are becoming popular in recent decades in understanding stellar structure and evolution. The binarity provides us with accurate ways to measure the physical parameters of the system and the component stars, meanwhile the oscillations offer us significant insight into their interiors as well as opportunities to probe the physics behind the pulsation nature of stars. The pulsating stars in eclipsing binaries have been noted since the early 1970s (Tempesti 1971; Broglia & Marin 1974, McInally & Austin 1977). Thanks to the space missions CoRoT (Baglin et al. 2006), Kepler (Borucki et al. 2010), and TESS (Ricker et al. 2015), a large number of eclipsing binaries with pulsating components were detected (Liakos & Niarchos 2017; Kahraman Aliçavuş et al. 2017, 2022; Gaulme & Guzik 2019; Shi et al. 2022). Among them, there are various types of pulsating stars, such as δ Scuti stars, γ Doradus stars, red giants, β Cephei stars, and Maia stars. Due to the relatively short periods and large amplitudes (Aerts et al. 2010), the δ Scuti stars in eclipsing binaries are a very useful type of variable. The δ Scuti variables are a class of late A- and early F-type stars that mainly pulsate with

low-order radial and nonradial modes in the range of 0.3 to 8 hours (Aerts et al. 2010). The δ Scuti-type stars in eclipsing binaries show similar pulsation characteristics to those of single stars, but the mass transfer between the two component stars makes them very distinct evolutionary histories. Up to now, there are about 350 δ Scuti pulsators identified in eclipsing binaries (Liakos & Niarchos 2017; Kahraman Aliçavuş et al. 2017, 2022; Gaulme & Guzik 2019; Shi et al. 2022).

During the last two decades, numerous studies focused on pulsating stars in eclipsing binaries have been carried out, especially for the δ Scuti variables. Kahraman et al. (2017) compared the δ Scuti-type pulsators in eclipsing binaries with the single stars and found that the binary components pulsate at shorter periods and lower amplitudes than those of single δ Scuti pulsators. Furthermore, relationships between the pulsation periods, amplitudes, and stellar parameters have been investigated (Soydugan et al. 2006; Liakos et al. 2012; Zhang et al. 2013; Kahraman Aliçavuş et al. 2017; Liakos & Niarchos 2017), where the well-known correlation is between the dominant pulsation period P_{dom} and orbital period P_{orb} . Zhang et al.(2013) presented a theoretical explanation for this relationship, and they derived the upper limit value of the $P_{\text{dom}}/P_{\text{orb}}$ ratio for the δ Scuti pulsators in eclipsing binaries to be 0.09 ± 0.02 . Moreover, some detailed studies of the δ Scuti variables in eclipsing binaries have made attempts to understand the interiors of the stars (Guo et al. 2017; Bowman et al. 2019; Chen et al. 2020, 2021). Guo et al. (2017) analyzed the post-mass-transfer binary KIC 9592855 and reported that the core and envelope of the pulsating component rotate nearly uniformly with its orbital motion. By combining observed properties with detailed models, Chen et al. (2020) found the Algol system KIC 10736223 had just undergone the rapid mass-transfer stage, and Chen et al.(2021) presented that OO Dra is an Algol-type binary formed through a helium-poor mass accretion. Therefore, the eclipsing binaries with pulsation components are crucial and very promising systems that offer us the opportunity to understand the intrinsic nature of pulsations and refine the theory of stellar structure and evolution.

Asteroseismology has been included as an important research subject in the project of the new space mission China Space Station Telescope (CSST). Thus, we search for stellar pulsators in eclipsing binaries based on the TESS data to obtain a more complete database. Since a large amount of the objects are observed only once by TESS, we focus on eclipsing binary with $P_{\text{orb}} < 13$ days from the catalogs of Prša et al. (2022), Shi et al. (2022), and Ding et al. (2022), and finally obtain a total of 6431 systems from the three catalogs. In this work, we aim to decipher whether there are δ Scuti variables in the TESS eclipsing binaries or not. In Section 2, we introduce the observation data and our scheme of target selection. We discuss the pulsation properties of the candidate targets in Section 3 and summarize our main results in Section 4.

2. OBSERVATIONS AND TARGET IDENTIFICATION

For the 6431 eclipsing binaries, we downloaded the 2-minute cadence photometric data from sectors 1-50 from the TESS Asteroseismic Science Operations Center (Tasoc, https://tasoc.dk/search_data/). From the files, we adopted the BJD times and the "PDCSAP_FLUX" flux corrected for instrumental trends through the Pre-search Data Conditioning Pipeline (Jenkins et al. 2016). Afterward, we removed outliers and normalized the flux with the methods described in Slawson et al. (2011). For stars located in overlapped sectors, we calculated the noises of their light curves with the method in Ding et al.(2022) and adopted the data with the minimum noise for further analyses.

For each eclipsing binary, three steps are included to test whether there is a pulsating component in the eclipsing binary or not. The details are as follows.

Firstly, we should eliminate the changes due to eclipses from the original data. The phase of the minimum flux corresponds to the moment of the primary minimum, and the orbital period is recalculated with the method described in Ding et al. (2022) to obtain a more precise period. We computed phases and folded the light curve as illustrated in Figure 1, and then obtained the pulsation light variations by subtracting the mean curve from the folded light curve (Chen et al. 2021). In this work, 500 bins in phase are used for all the 6431 eclipsing binaries. In Figure 1, the mean light curve is shown with the red line in the top panel and the light residuals in plots of magnitude versus phase shown in the middle panel.

Secondly, we use the Lomb-Scargle algorithm for the light residuals and show the amplitude spectrum in the bottom panel of Figure 1. Since δ Scuti stars pulsate mainly in low-order p modes with periods in the range 0.3 to 8 hours, thus we carried out further frequency analysis in the range $0\text{-}100 \text{ day}^{-1}$. In order to remove the harmonics of the orbital frequency, we generate a series of orbital-harmonic peaks n/P_{orb} , where n varies from 1 to the integer nearest to $100/P_{\text{orb}}$. We set their amplitudes to be a fixed value (the maximum amplitude of the amplitude spectrum) and the frequency resolution $1.5/\Delta T$ (Loumos & Deeming 1978) to be the uncertainties of those orbital-harmonic peaks. We

divided the amplitude spectrum by the orbital-harmonic peaks and finally obtained a pure amplitude spectrum due to intrinsic pulsations. We show the amplitude spectrum with black lines and mark the peaks that can be eliminated by the orbital harmonics with the gray lines in the bottom panel of Figure 1.

Finally, as suggested by Breger et al. (1993) and Baran et al. (2015), the empirical threshold of the signal-to-noise ratio is $S/N = 4$ and 5.4 for a frequency that is accepted to be a signal, respectively. In this work, we adopt a moderate value $S/N = 5$ and denoted the criteria with the dotted line in the bottom panel of Figure 1. The noise is calculated in the range of 2 day^{-1} around each frequency.

We examine the pulsation amplitude spectrum for each target using the criteria of whether peaks with $S/N > 5$ are detected or not, and find 242 candidate δ Scuti variables in eclipsing binaries. Therein, 143 targets are new discoveries. We list their parameters in Table 1 and present their amplitude spectra in Figure 2.

3. PROPERTIES OF THE PULSATINg STARS IN ECLIPSING BINARIES

In this section, we examine the properties of the 242 candidate δ Scuti variables in eclipsing binaries. For 229 stars, there are stellar atmospheric parameters provided in the TESS input catalog, while 189 objects were also observed by Gaia (Gaia Collaboration 2022). Figures 3 and 4 present positions of the 189 targets in the Hertzsprung-Russell diagram. In the figures, the luminosities L from Gaia DR3 are adopted, while the effective temperatures T_{eff} from the TESS input catalog are used in Figure 3 and T_{eff} from Gaia DR3 are used in Figure 4. It can be seen in Figure 3 that most of the targets are located in the δ Scuti instability strip except for TIC 125754991, TIC 165310952, and TIC 326356701, while many targets are beyond the blue edge of the instability strip in Figure 4. According to the work of Uytterhoeven et al.(2011), the typical T_{eff} of δ Scuti stars ranges from 6000 K to 9000 K. TIC 326356701 with $T_{\text{eff}} = 4674 \text{ K}$ and $\log g = 1.5484$ can be a pulsating red giant. For TIC 125754991 and TIC 165310952, we find them hotter than δ Scuti stars but cooler than β Cephei stars and their oscillations in the range of δ Scuti stars, thus we suggest them to be two Maia variables.

Figure 5 depicts the $P_{\text{dom}}\text{-}P_{\text{orb}}$ diagram for the 242 targets. In the figure, most of the targets manifest a consistent distribution trend with the theoretical relation derived by Zhang et al.(2013). And we also notice that 9 objects significantly exceed the upper limit of the $P_{\text{dom}}/P_{\text{orb}}$ ratio given by Zhang et al.(2013), including TIC 101531285, TIC 220511367, TIC 440459327, TIC 19193162, TIC 141622065, TIC 262958558, TIC 304030311, TIC 431555426, and TIC 449486448. In this work, we discover six new pulsating stars in eclipsing binaries with $P_{\text{orb}} < 0.65$ days and display their amplitude spectra in Figure 6. As shown in Figure 6, all the six targets exhibit δ Scuti-type pulsations, which may indicate that P_{dom} and P_{orb} are uncorrelated for eclipsing binaries with $P_{\text{orb}} < 0.65$ days. For TIC 19193162, TIC 141622065, TIC 262958558, TIC 304030311, TIC 431555426, and TIC 449486448, their amplitude spectra in Figure 7 suggest them to be γ Doradus- δ Scuti hybrid stars.

Maia stars and β Cephei stars are two groups of pulsating stars whose frequencies resemble δ Scuti variables (Aerts et al. 2010; Balona & Ozuyar 2020). Combining parameters in Table 1 and their amplitude spectra, TIC 315777432 may be another Maia star. Balona & Ozuyar (2020) reported that T_{eff} of most β Cephei stars are higher than 18000 K and their dominant frequencies exceed 2.5 d^{-1} . TIC 30562668, TIC 50897998, TIC 60433558, TIC 91111448, and TIC 335265326 are five likely β Cephei variables. Therein, TIC 30562668, TIC 60433558, TIC 91111448, and TIC 335265326 are newly discovered stars. Besides, we suggest TIC 148560397, TIC 229742425, TIC 266006310, and TIC 339570153 to be four δ Scuti- γ Doradus hybrid stars, and TIC 316633520, TIC 330658205, TIC 337886863, TIC 396134795, and TIC 396201681 to be five γ Doradus- δ Scuti hybrid stars. TIC 138893145 and TIC 229771234 are two cool stars of unknown type. Gaulme & Guzik (2019) classified TIC 138893145 to be a pulsating red giant or a triple system. TIC 229771234 is an unclassified star. Its $\log g$ from the TESS input catalog is 4.4 dex and its frequencies seem to exhibit uniformly-spaced behaviors.

Finally, 216 targets are identified as pure δ Scuti stars. Barceló Forteza et al. (2018) and (2020) presented a relation between the dominant frequency and the effective temperature. The distribution of the eclipsing binaries with δ Scuti variables within the $T_{\text{eff}}\text{-}\nu_{\text{dom}}$ diagram are depicted in Figure 8. In the figure, we adopt T_{eff} from the TESS input catalog and find that almost all targets are consistent with the relationship except for TIC 280723146. The effective temperature T_{eff} of TIC 280723146 from the TESS input catalog is 5711 K and 7290 K from Gaia DR3, thus we still classify it as a δ Scuti star. Figure 9 plots the histogram of the dominant pulsation frequencies of the δ Scuti stars in eclipsing binaries. In the figure, there is a maximum value of the population of stars at $225 \mu\text{Hz}$, which is similar to the result of δ Scuti single stars in Barceló Forteza et al.(2020). Moreover, we found that the proportion of stars in the total number at the high-frequency region is significantly higher than that of single stars. Our result could be

ascribed to the mass transfer process between the two components. Due to the mass transfer, the mass of the pulsating component increases at decreasing periods.

4. CONCLUSIONS

In this work, we present the results of our search for pulsating components in 6431 eclipsing binaries observed by TESS in the 2-minute cadence photometric data from sectors 1-50. After eliminating the changes due to eclipses and the orbital-harmonic peaks, we found 242 binaries showing pulsation signals, of which 143 objects are new discoveries.

Then we discuss the pulsation properties of our candidate targets based on the H-R diagram and the well-known relations between the pulsation period ν_{dom} and other parameters, such as the $P_{\text{dom}}-P_{\text{orb}}$ relation and the $\nu_{\text{dom}}-T_{\text{eff}}$ relation. Among the 242 targets, 216 stars are recognized to be δ Scuti stars (123 new), 11 γ Doradus- δ Scuti hybrid stars (8 new), 5 β Cephei stars (4 new), 4 δ Scuti- γ Doradus hybrid stars (3 new), 3 Maia stars (3 new), 2 pulsating red giants (1 new), and a new unclassified star. As for the six systems with $P_{\text{orb}} < 0.65$ days, 3 of which significantly exceed the upper limits of the $P_{\text{dom}}/P_{\text{orb}}$ ratio. However, all the 6 targets show normal δ Scuti-type pulsations. This feature may suggest that P_{dom} and P_{orb} are uncorrelated for eclipsing binaries $P_{\text{orb}} < 0.65$ days.

We statistically analyze the dominant pulsation modes of the 216 δ Scuti stars in eclipsing binaries. Compared with the distribution of dominant pulsation frequencies for single δ Scuti stars, there is a similar maximum value of the population of stars around 225 μHz . Besides, we find the proportion of stars in eclipsing binaries at the high-frequency region significantly higher than that of single stars. This result may indicate that those binaries form in different mechanisms. The mass transfer makes the mean density of the mass accretors increase and its pulsation period decrease. Such a subject will be explored in future work.

Finally, the paper provides a vast sample of eclipsing binaries with pulsating components, which will allow for a significant improvement of the knowledge on the stellar structure and evolution and will help to understand the characteristics of pulsations in eclipsing binaries. More spectroscopic and photometric observations will be required in the future to determine their fundamental stellar parameters and constrain evolutionary models.

We are sincerely grateful to the anonymous referee for instructive advice and productive suggestions. This work is supported by the National Key R&D Program of China (Grant No.2021YFA1600400/2021YFA1600402) and by the B-type Strategic Priority Program No. XDB41000000 funded by the Chinese Academy of Sciences. The authors also appreciate supports of the National Natural Science Foundation of China (grant NO. 12173080 and 12288102 to X-H.C., 12103088 to X.D., 11833002 and 11973053 to X-B.Z., 12133011 and 12288102 to Y.L.). X-H.C. also sincerely acknowledges the supports of the Yunnan Revitalization Talent Support Program Young Talent Project, the Yunnan Fundamental Research Projects (202101AT070006), the science research grants from the China Manned Space Project with NO. CMS-CSST-2021-B07, and the West Light Foundation of the Chinese Academy of Sciences. L-T.C. acknowledges the support of the Natural Science Foundation of Shandong Province (ZR2021QA105). X-B.Z. also acknowledges the support of Sichuan Science and Technology Program (2020YFSY0034). X-Z.L. acknowledges the project funded by China Postdoctoral Science Foundation (2021M703099). This paper includes data collected by the TESS mission and obtained from the TESS Asteroseismic Science Operations Center (Tasoc). This paper also uses data from the European Space Agency (ESA) space mission Gaia (<https://www.cosmos.esa.int/gaia>), processed by the Gaia Data Processing and Analysis Consortium (DPAC, <https://www.cosmos.esa.int/web/gaia/dpac/consortium>). Funding for the DPAC is provided by national institutions, in particular the institutions participating in the Gaia MultiLateral Agreement. The authors sincerely acknowledge them for providing such excellent data.

REFERENCES

- Aerts, C., Christensen-Dalsgaard, J., & Kurtz, D. W. 2010, *Asteroseismology, Astronomy and Astrophysics Library*. ISBN 978-1-4020-5178-4. Springer Science+Business Media B.V., 2010, p
- Baglin, A., Auvergne, M., Barge, P., et al. 2006, *The CoRoT Mission Pre-Launch Status - Stellar Seismology and Planet Finding*, 1306, 33
- Balona, L. A. & Ozuyar, D. 2020, *MNRAS*, 493, 5871
- Baran, A. S., Koen, C., & Pokrzywka, B. 2015, *MNRAS*, 448, L16
- Barceló Forteza, S., Roca Cortés, T., & García, R. A. 2018, *A&A*, 614, A46
- Barceló Forteza, S., Moya, A., Barrado, D., et al. 2020, *A&A*, 638, A59

- Borucki, W. J., Koch, D., Basri, G., et al. 2010, *Science*, 327, 977
- Bowman, D. M., Johnston, C., Tkachenko, A., et al. 2019, *ApJL*, 883, L26
- Breger, M., Stich, J., Garrido, R., et al. 1993, *A&A*, 271, 482
- Broglia, P. & Marin, F. 1974, *A&A*, 34, 89
- Chen, X. H., Zhang, X. B., Li, Y., et al. 2020, *ApJ*, 895, 136
- Chen, X. H., Zhang, X. B., Li, Y., et al. 2021, *ApJ*, 920, 76
- Cui, K. M., Guo, Z., Gao, Q., et al. 2020, *ApJ*, 898, 136
- Ding, X., Ji, K. F., Li, X. Z., et al. 2022, *PASJ*, submitted
- Doğruel, M. B. & Gürol, B. 2015, *NewA*, 40, 20
- Gaia Collaboration 2022, *VizieR Online Data Catalog*, I/355
- Gaulme, P., McKeever, J., Rawls, M. L., et al. 2013, *ApJ*, 767, 82
- Gaulme, P. & Guzik, J. A. 2019, *A&A*, 630, A106
- Guo, Z., Gies, D. R., & Matson, R. A. 2017, *ApJ*, 851, 39
- Hasanzadeh, A., Safari, H., & Ghasemi, H. 2021, *MNRAS*, 505, 1476
- Holdsworth, D. L., Smalley, B., Gillon, M., et al. 2014, *MNRAS*, 439, 2078
- Hong, K., Lee, J. W., Koo, J.-R., et al. 2017, *AJ*, 153, 247
- Jenkins, J. M., Twicken, J. D., McCauliff, S., et al. 2016, *Proc. SPIE*, 9913, 99133E
- Kahraman Aliçavuş, F., Soydugan, E., Smalley, B., et al. 2017, *MNRAS*, 470, 915
- Kahraman Aliçavuş, F., Gümüş, D., Kirmızıtaş, Ö., et al. 2022, *Research in Astronomy and Astrophysics*, 22, 085003
- Kim, S. L., Lee, J. W., Youn, J.-H., et al. 2002, *A&A*, 391, 213
- Kim, S. L., Lee, J. W., Lee, C.-U., et al. 2010, *PASP*, 122, 1311
- Lee, J. W., Hong, K., Koo, J.-R., et al. 2018, *AJ*, 155, 5
- Lee, J. W., Kristiansen, M. H., & Hong, K. 2019, *AJ*, 157, 223
- Lehmann, H., Southworth, J., Tkachenko, A., et al. 2013, *A&A*, 557, A79
- Li, Y. & Stix, M. 1994, *A&A*, 286, 815
- Liakos, A., Niarchos, P., Soydugan, E., et al. 2012, *MNRAS*, 422, 1250
- Liakos, A. & Niarchos, P. 2017, *MNRAS*, 465, 1181
- Liakos, A. 2020, *A&A*, 642, A91
- Loumos, G. L. & Deeming, T. J. 1978, *Ap&SS*, 56, 285
- McInally, C. J. & Austin, R. D. 1977, *Information Bulletin on Variable Stars*, 1334, 1
- Miszuda, A., Szewczuk, W., & Daszyńska-Daszkiewicz, J. 2021, *MNRAS*, 505, 3206
- Miszuda, A., Kołaczek-Szymański, P. A., Szewczuk, W., et al. 2022, *MNRAS*, 514, 622
- Mkrtychian, D. E., Lehmann, H., Rodríguez, E., et al. 2018, *MNRAS*, 475, 4745
- Paxton, B., Bildsten, L., Dotter, A., et al. 2011, *ApJS*, 192, 3
- Paxton, B., Cantiello, M., Arras, P., et al. 2013, *ApJS*, 208, 4
- Paxton, B., Marchant, P., Schwab, J., et al. 2015, *ApJS*, 220, 15
- Paxton, B., Schwab, J., Bauer, E. B., et al. 2018, *ApJS*, 234, 34
- Prša, A., Kochoska, A., Conroy, K. E., et al. 2022, *ApJS*, 258, 16
- Rappaport, S. A., Kurtz, D. W., Handler, G., et al. 2021, *MNRAS*, 503, 254
- Ricker, G. R., Winn, J. N., Vanderspek, R., et al. 2015, *Journal of Astronomical Telescopes, Instruments, and Systems*, 1, 014003
- Rodríguez, E., García, J. M., Costa, V., et al. 2010, *MNRAS*, 408, 2149
- Shi, X. D., Qian, S. B., & Li, L. J. 2022, *ApJS*, 259, 50
- Slawson, R. W., Prša, A., Welsh, W. F., et al. 2011, *AJ*, 142, 160
- Stassun, K. G., Oelkers, R. J., Paegert, M., et al. 2019, *AJ*, 158, 138
- Southworth, J., Zima, W., Aerts, C., et al. 2011, *MNRAS*, 414, 2413
- Southworth, J., Bowman, D. M., & Pavlovski, K. 2021, *MNRAS*, 501, L65
- Soydugan, E., İbanoğlu, C., Soydugan, F., et al. 2006, *MNRAS*, 366, 1289
- Streamer, M., Ireland, M. J., Murphy, S. J., et al. 2018, *MNRAS*, 480, 1372
- Tempesti, P. 1971, *Information Bulletin on Variable Stars*, 596, 1
- Wang, K., Zhang, X. B., & Dai, M. 2020, *ApJ*, 888, 49
- Xiong, D. R., Deng, L., Zhang, C., et al. 2016, *MNRAS*, 457, 3163
- Zhang, X. B., Luo, C. Q., & Fu, J. N. 2013, *ApJ*, 777, 77
- Zhang, X. B., Deng, L. C., Tian, J. F., et al. 2014, *AJ*, 148, 106
- Zhang, X. B., Luo, Y. P., & Wang, K. 2015, *AJ*, 149, 96

Table 1. Parameters of the systems that exhibit pulsations.

TIC	R.A.	Decl.	T_{mag}	P_{orb}	P_{dom}	$T_{\text{eff}}^{\text{TESS}}$	$\log g^{\text{TESS}}$	$T_{\text{eff}}^{\text{Gaia}}$	$\log g^{\text{Gaia}}$	L^{Gaia}	Etype	Ptype	New PB	Literature
	(degree)	(degree)	(mag)	(day)	(day)	(K)	(dex)	(K)	(dex)	(L_{\odot})				
737546	74.5150265728	-29.9330102960	10.5401	3.06745	0.058525	7068	3.4795	7269	3.6592	27.83	EB	δ Sct		SHI22
3965274	12.7806766130	-11.1421801122	11.5730	0.97593	0.017224	8079	4.2141	7992	3.8997	11.19	EW	δ Sct		HOL14
7854182	275.5486470640	47.5688780672	9.0619	0.86605	0.019993	7424	4.1549	7665	4.0699	10.59	EB	δ Sct		KAH17,LIA17
8669966	248.3713500555	30.4990669191	6.6493	3.39333	0.073412	7651	3.5436				EW	δ Sct		KAH22
9473243	258.3973578307	30.7100119195	10.5583	2.26697	0.056450	7093	4.0218	7553	4.0217	12.51	EA	δ Sct		KAH17,LIA17
15613315	16.3017024552	27.7675410431	9.6207	0.71665	0.061124	7288	4.0251	7251	3.9698	11.71	EB	δ Sct	Y	
17336666	65.9143623230	21.3388350724	10.9929	2.95560	0.085187	7162					EA	δ Sct		SHI22
19193162	123.7982557439	-6.3150231583	8.8788	5.69178	0.586438	7213	3.5239	7286	3.8491	36.46	EA	γ Dor- δ Sct	Y	
25195864	63.7535635637	-69.5366740145	10.4614	0.74310	0.037396	7523	3.7231	8480	3.9305	26.06	EW	δ Sct		LIA17,HAS21,BAR20
27844498	296.4906728723	50.9058605667	11.1924	4.42263	0.042329	7722	3.5715	8233	3.6902	54.91	EB	δ Sct		GAU19,CUI20
30562668	134.2814668951	-43.2561965581	5.9917	3.85081	0.114486			18535	3.3004		EB	β Cephei	Y	
31653503	46.3510299657	-66.6842455537	10.9399	6.68132	0.044933	6328	3.4838				EB	δ Sct	Y	
33834253	63.7226832666	-73.3604122895	11.4218	3.23223	0.110378	7140	3.6121	7316	3.6851	27.42	EA	δ Sct	Y	
35743561	39.8967084115	-0.2622725567	11.4065	2.72087	0.048913	7312	3.7668				EA	δ Sct	Y	
37601240	93.1552150914	-25.2687352643	8.9637	0.73136	0.055867	7588	4.2383	7498	4.0530	8.28	EB	δ Sct	Y	
37817410	65.4180442859	-6.0192226525	9.2920	2.60558	0.053428	7208	3.9892	7513	3.8938	13.86	EA	δ Sct		KAH17,LIA17,MKR18
39011225	118.1668468136	39.5383071699	7.1290	2.62881	0.184302	7299	3.6066	7263	3.5214	42.36	EA	δ Sct	Y	
45294109	92.3326604364	18.2892200995	13.8980	0.36871	0.034239	7522	4.2476	7979	4.1483	10.96	EB	δ Sct	Y	
45918336	149.8182437551	-41.2567359178	11.2302	2.14013	0.059731	8116	4.0187	7813	3.9173	15.54	EA	δ Sct	Y	
48084398	281.8732458071	49.4320228548	6.8446	4.24361	0.084129	6814	3.2927	6862	3.2650	46.15	EB	δ Sct		SHI22,KAH22
48188257	282.5472100339	48.8564066458	12.7756	2.19167	0.015520	8455	4.3322	9826	4.1969	32.28	EB	δ Sct		KAH17,LIA17
48335665	148.4483941173	-34.5755893123	10.8358	4.62865	0.052979	7098	3.5137	7526	3.7119	31.50	EB	δ Sct	Y	
49418981	173.5889674270	-5.5270999772	6.4563	2.56768	0.081647	7065	3.8700	7058	3.8861	12.47	EB	δ Sct	Y	
49677785	351.4492469005	-11.6098951832	9.3994	1.59350	0.038212	7844	3.8395	7793	3.7813	24.94	EB	δ Sct		KAH17,LIA17
50897998	83.3810301673	-1.1560720853	5.6058	1.48544	0.108923			18266	3.6312		EB	β Cephei		SOU21
54001270	33.15410008798	-29.5484314480	10.6142	2.34922	0.041326	7816	3.7103	9072	3.9783	54.80	EA	δ Sct		SHI22
54018297	23.8996325029	-11.9418511853	8.8591	1.93980	0.075692	7174	3.8369	7278	3.8059	16.84	EA	δ Sct		KAH17,LIA17
56127811	70.7799489497	-7.4116931399	9.1365	3.72351	0.020059						EA	δ Sct		SHI22
60433558	273.6755785367	-33.1408936644	8.6390	10.80533	0.147444			23757	3.8023		EA	β Cephei	Y	
61386324	24.2116340924	33.6599179837	8.3493	0.73161	0.050628	7735	4.1911				EB	δ Sct	Y	
63328020	320.0600083621	51.3947270718	11.5528	1.10577	0.049524	7106	3.5961	8045	3.7595	37.87	EB	δ Sct		RAP21
64437380	235.6983502812	-57.5109483965	9.8962	2.34694	0.033737	7030	3.6749				EB	δ Sct	Y	
65448527	41.9307680380	-25.2636867300	12.1112	0.66781	0.029259	8116	4.4009	8109	4.2132	7.18	EB	δ Sct	Y	
68032870	219.3472146728	38.0782749673	10.8881	1.03337	0.026823	7566	4.0869	7436	3.9088	11.58	EB	δ Sct	Y	
68144913	279.7729924679	32.2562306289	11.4431	0.65276	0.025305	7790	4.2305	8023	4.0912	11.56	EB	δ Sct	Y	
71103363	91.9248616399	60.8017374112	11.8468	2.44863	0.020143	8176	4.2214				EA	δ Sct	Y	
73672504	155.5980747959	-39.7453798220	10.8227	3.00204	0.117678	7306	3.3123	7284	3.4575	38.80	EA	δ Sct		SHI22
74627376	137.9263152802	-46.8862277885	8.5690	2.61257	0.110000			7444	3.3223	274.90	EB	δ Sct		SHI22
75593781	85.3956201214	25.9980520192	11.4351	1.53207	0.019261	8300	4.3274				EA	δ Sct		KAH22
78148497	88.6019516828	26.3087982961	10.8176	2.70994	0.080356	7287	3.9326	7337	3.8903	13.39	EB	δ Sct		SHI22,KAH22
79931363	120.8536726194	-42.1877992595	9.7813	0.71572	0.035921	7865	4.1273	7189	3.8873	8.89	EB	δ Sct	Y	
80259373	7.1696308623	-44.6245691991	10.9776	0.63297	0.013047	8543	4.5955	9155	4.3856	9.59	EB	δ Sct	Y	
81038220	123.4914514739	57.2659514951	10.2772	2.02227	0.027026	7526	4.0659	7955	3.9565	13.73	EA	δ Sct		LIA12
83833793	217.4650186377	-24.7242719501	10.5126	2.17359	0.051926	7469		8094	3.8313	15.46	EA	δ Sct	Y	
83914837	218.0213405202	-27.7091388555	7.2435	0.91181	0.030779	7373	4.1943				EB	δ Sct	Y	
85600400	259.2082390246	38.3662920672	11.8024	1.47224	0.094558	7236	3.8548	7239	3.7645	20.31	EB	δ Sct		KAH22

Table 1 continued on next page

Table 1 (*continued*)

TIC	R.A.	Decl.	T_{mag}	P_{orb}	P_{dom}	$T_{\text{eff}}^{\text{TESS}}$	$\log g^{\text{TESS}}$	$T_{\text{eff}}^{\text{Gaia}}$	$\log g^{\text{Gaia}}$	L^{Gaia}	Etype	Ptype	New PB	Literature
	(degree)	(degree)	(mag)	(day)	(day)	(K)	(dex)	(K)	(dex)	(L_{\odot})				
91111448	302.0961322613	35.4592994638	9.1127	1.70663	0.075644			18095	4.0732		EB	β Cephei	Y	
91369561	312.5682800170	-42.2179438251	10.9545	3.98319	0.073957	7105	3.6456				EB	δ Sct		LIA17
93059429	52.7119951153	-13.9240825650	11.6423	1.48150	0.037265	7923	3.9162	8109	3.9120	20.33	EB	δ Sct	Y	
95196329	115.7817482727	-11.1876530355	11.7018	0.90044	0.064591	7401	3.8576	7482	3.8012	23.55	EB	δ Sct	Y	
97467902	23.5765287783	-27.3631260780	7.6318	2.04459	0.037118	7518	3.7241				EB	δ Sct		SHI22
101531285	150.2554823558	-34.2920015279	8.9634	0.30363	0.066088	7224	4.0989	7130	3.9395	8.62	EW	δ Sct	Y	
116334565	85.1182200638	30.9742414837	11.1125	3.47256	0.087486	7546	3.5978				EA	δ Sct		KAH22
116502572	233.8679514412	43.4803236981	11.3452	3.93223	0.061231	6533	3.5881	10814	4.1835	79.80	EB	δ Sct		KAH17,LIA17
120414806	0.1250822145	-39.6247622077	10.7026	2.55280	0.022153	7450	4.0020	7813	3.9295	15.49	EA	δ Sct	Y	
121078334	56.5986922922	-21.9721043002	9.3429	0.92850	0.056547	7421	4.1354	7361	3.9847	10.34	EB	δ Sct	Y	
121420805	341.8335368235	-47.9160719778	11.3169	1.71701	0.016553	7942	4.2016				EA	δ Sct	Y	
123042728	279.1897869675	43.2218153400	5.9804	1.31265	0.055963	7463	3.4943	7315	3.5420	39.59	EB	δ Sct	Y	
123042744	279.2049048766	43.2433834268	11.1032	1.31257	0.052912	6562	4.2576	6410	4.1271	3.30	EB	δ Sct	Y	
124688144	93.72112128251	-33.0731932350	10.6762	1.24618	0.022549	8088	4.3038	8387	4.1635	11.12	EA	δ Sct	Y	
125498216	105.7125753163	-11.7655945106	9.6543	0.71388	0.022741	8088	4.3136	7992	4.0686	9.21	EB	δ Sct	Y	
125754991	58.8727233330	24.2883380526	6.7792	2.46116	0.045673	9962	4.1123	11109	4.1204	64.71	EA	Maia	Y	
126137581	110.2637797680	25.6688239111	8.5546	1.04775	0.028804	7723	4.2911	7578	4.1499	7.67	EB	δ Sct	Y	
126321739	134.9424464858	25.8552012732	12.7968	0.79195	0.028574	7976	4.2233	8317	4.1161	17.86	EB	δ Sct	Y	
126602778	314.5087578290	-46.0667710152	10.8078	0.71213	0.057894	7454	4.0993	7522	4.0053	12.19	EB	δ Sct	Y	
126945917	318.7323618732	-43.3954476169	9.1063	1.34107	0.045304	7580	3.9855	7466	3.9221	14.75	EA	δ Sct		SHI22
129764561	35.4020502946	-37.2126901064	9.9395	2.43471	0.039613	7527	3.8513	10216	4.1493	47.34	EA	δ Sct	Y	
129861919	55.5501519986	-38.4968177266	10.3862	0.70142	0.050858	6634					EB	δ Sct	Y	
138893145	294.9363790779	39.8524649894	10.1526	3.75067	0.162226	4580					EB	RGB or Triple		GAU13, GAU19
139701741	66.3967470206	-18.8005583916	11.6864	2.62979	0.059128	7117	3.8023	7677	3.9156	13.24	EB	δ Sct		SHI22
141622065	89.2287416960	-73.3426393715	9.7993	2.92792	0.377136	6640	3.4682	6861	3.6511	22.56	EB	γ Dor- δ Sct	Y	
144462697	336.3483090293	-44.5942263579	11.8315	1.23401	0.043803	7337	4.2078	7561	4.1148	8.00	EA	δ Sct	Y	
147201138	322.9532248197	-45.0450932242	10.9686	1.88051	0.030262	7551	3.8885	8114	3.9060	21.96	EA	δ Sct		BOW19
148559140	164.2816735605	-6.2733533494	9.7805	0.82563	0.023435	7891	4.2133				EB	δ Sct	Y	
148560397	164.3776019933	-11.0879926170	8.9136	1.35017	0.056870						EA	δ Sct- γ Dor	Y	
149160359	81.4550908276	-64.9893744768	9.9927	1.12082	0.036331	7931	3.9159	7894	3.9102	20.34	EB	δ Sct		WK20
150443185	97.8678805718	-63.5353762050	9.4343	2.59376	0.021750	7421	3.9282	7500	3.9310	16.46	EA	δ Sct	Y	
152223725	312.2794999388	-33.7317933625	9.3148	4.43644	0.081727	7708	3.4433	9390	3.7611	113.80	EA	δ Sct		KAH17,LIA17
152513129	172.1072965932	-39.7298573935	12.0743	4.12675	0.020192	7575	4.0418	9842	4.2509	26.82	EB	δ Sct	Y	
157273321	198.7268625502	59.2956675972	7.8863	5.51960	0.059238	7285	3.5397	10352	3.8798	111.00	EB	δ Sct		KAH17,LIA17
158794976	288.7183567756	42.5022843106	9.9366	0.77267	0.036402	7510	4.0154	7462	3.9550	12.82	EW	δ Sct		SHI22
159298033	229.4895851838	83.8594649404	7.3670	1.72499	0.055414	7204	4.0067	7329	3.8972	11.88	EB	δ Sct	Y	
159638876	317.7559917720	-40.5393026742	8.1990	2.39299	0.091245	7089	3.5983	6956	3.6509	24.36	EB	δ Sct	Y	
159864583	221.4063516221	-40.0303761311	8.5822	3.63856	0.162635	6991	3.8801	6885	3.8322	11.83	EB	δ Sct	Y	
160036449	336.7522882506	-37.1883684346	10.8022	1.89317	0.020405	7517	4.0996				EA	δ Sct		SHI22
160081043	352.0531716144	-39.9232510262	12.9518	0.76866	0.045813	7800	4.3552	7936	4.2609	7.26	EB	δ Sct	Y	
163008999	242.3037019576	-43.1986572213	9.6266	1.85412	0.106766	6850	3.6464				EA	δ Sct		
164646288	283.9097468481	42.1310107932	10.5013	0.73378	0.042476	7448	4.1086	7692	4.0132	12.74	EB	δ Sct		KAH17,LIA17
165310952	299.2429420462	54.7995223834	8.4462	1.80517	0.131684	9103		10618	3.7124	240.90	EB	Maia	Y	
165459595	180.1920401708	-40.3545012557	9.3150	3.33691	0.046010	7697	4.0832	7470	3.9615	12.25	EA	δ Sct		SHI22
165618747	260.0324962828	13.6660148220	11.4332	0.64823	0.026403	7603	4.1085	8308	4.1310	13.96	EB	δ Sct		KAH22
166874908	59.6597216407	-31.2772956509	10.1725	2.18916	0.039400	7635		7802	3.9464	33.75	EB	δ Sct	Y	
169168102	127.1214720000	-2.5171730000	6.1070	2.49973	0.029610						EA	δ Sct		BAR20
169532543	78.0438100581	-13.1996046163	9.7605	0.91541	0.031379	7928	4.0117	10051	4.2255	37.32	EB	δ Sct		KAH17,LIA17

Table 1 continued on next page

Table 1 (*continued*)

TIC	R.A.	Decl.	T_{mag}	P_{orb}	P_{dom}	$T_{\text{eff}}^{\text{TESS}}$	$\log g^{\text{TESS}}$	$T_{\text{eff}}^{\text{Gaia}}$	$\log g^{\text{Gaia}}$	L^{Gaia}	Etype	Ptype	New PB	Literature
	(degree)	(degree)	(mag)	(day)	(day)	(K)	(dex)	(K)	(dex)	(L_{\odot})				
172431974	299.7087813125	39.3311433479	10.5887	2.34477	0.187775	7236	3.7116				EA	δ Sct		KAH22
175405906	349.8565525181	-40.2906698848	11.3969	2.01250	0.054876	6920		7161	3.8331	18.53	EA	δ Sct	Y	
177283493	102.4684550367	-73.4007811676	11.8481	0.75281	0.052694	7278	3.9772	7753	3.9970	13.97	EB	δ Sct	Y	
178286775	60.6982435098	-18.8247670600	10.5348	1.12638	0.018187	7557	4.2620	7880	4.0876	8.97	EB	δ Sct	Y	
178996712	70.0633105020	-27.7350809463	8.5850	2.98205	0.034765	7188	4.1017	7282	4.0275	8.81	EB	δ Sct	Y	
181043970	12.9441610409	-71.9980354033	10.4156	0.87092	0.017011	8684	4.1875	8428	4.2379	14.28	EA	δ Sct	Y	
183143120	125.0177546163	-38.4098114462	11.3309	0.49390	0.027314	8312	4.3537				EB	δ Sct	Y	
184246521	295.8339922256	39.9522626606	10.7680	2.47025	0.052371	7753	3.5174	7594	3.4853	44.17	EB	δ Sct		GAU19,LIA20
184318481	127.0757311805	-38.9720322442	8.4729	1.55787	0.021267	7899	4.3156	8077	4.3044	9.02	EA	δ Sct	Y	
188630094	350.5857754196	-15.9390248074	10.4939	0.86275	0.030981	7354	3.9536	7415	3.9156	12.94	EB	δ Sct		KAH17,LIA17
193391232	305.7618343832	43.2423563160	10.4713	3.45091	0.031176	7681	3.8612				EA	δ Sct		KAH17,LIA17
193774939	268.3030649995	43.7731023005	9.8556	1.30579	0.046307	7358	4.0550	7506	3.9778	11.47	EA	δ Sct		KAH22
197757000	337.2080240079	53.7710780374	10.4189	2.20651	0.027283	6985	3.9230	10057	4.2701	36.06	EA	δ Sct		KAH22
198037741	61.6537070111	-56.5752786716	8.5467	0.78000	0.048889	7274	3.8397	7463	3.9550	12.93	EB	δ Sct	Y	
199688409	253.0514502264	57.7254690748	12.0490	0.86811	0.033204	7738	4.1345	7824	4.0069	13.03	EB	δ Sct	Y	
200440270	70.8966718559	-42.6758227821	10.1114	1.07885	0.016486	8123	4.1742	9793	4.1923	24.17	EB	δ Sct		BAR20
202299805	225.1608428572	57.7751470014	11.5680	1.54580	0.018534	7709	4.2172	7954	4.0748	9.24	EA	δ Sct	Y	
214330573	261.1089384280	-52.5672613424	9.2178	1.91207	0.092655	6662	3.5863				EB	δ Sct	Y	
217279153	260.1266540055	-43.0762219588	10.6201	1.60971	0.042121	7216	3.8748	7745	3.9741	15.20	EA	δ Sct		LIA17
218996233	124.7665718848	-18.5659931911	11.6094	0.77637	0.040478	7551	4.3347	7925	4.1870	7.15	EA	δ Sct	Y	
219373406	76.2354874222	-53.1405873748	10.5108	0.86189	0.019870	7766	4.0242	7933	4.0459	15.02	EB	δ Sct	Y	
219707463	136.5934902441	68.4451458176	6.8367	9.01513	0.045098	7541	3.9818				EA	δ Sct		SHI22
220402294	69.5598201448	-57.1921582692	11.2216	0.78521	0.028387	7258	4.0560	7279	3.9845	10.30	EB	δ Sct	Y	
220511367	347.4854084181	-54.6222138491	9.5287	0.31750	0.046722	7566	4.3053	7489	4.1765	6.53	EW	δ Sct	Y	
220962774	246.5646776038	-55.2088921324	9.2632	0.99449	0.047819	6821	3.8944	7318	3.9436	13.43	EB	δ Sct	Y	
229742425	279.7204436093	70.2315768197	10.3807	1.26528	0.049903	7260	4.1469	7364	4.0851	8.44	EB	δ Sct-γ Dor	Y	
229771234	282.2677475537	68.1569510253	10.7665	0.82092	0.047984	4000	4.4290				EB	unclassified	Y	
231714759	352.5927028842	-58.4262810043	9.3827	5.46147	0.030842	7087	3.6567	7571	3.7370	26.12	EB	δ Sct	Y	
231973885	95.5053539497	-47.8992013797	11.0410	2.89466	0.044452	7545	3.7785	9958	4.1059	63.44	EA	δ Sct		SHI22
232052561	97.3117988385	-45.8704641837	10.0244	3.01064	0.155260	7256	4.1364	7313	4.1212	8.04	EA	δ Sct	Y	
233195058	264.2695830000	67.1192300000	7.7650	2.67930	0.048528						EA	δ Sct	Y	
233291864	300.4182617987	58.0971758417	9.9607	2.68961	0.047421	8062	4.2450	7883	4.1491	10.18	EA	δ Sct	Y	
238607300	132.7133472298	19.3572963923	11.8142	1.32375	0.076777	7114	3.7702	7296	3.7998	20.95	EB	δ Sct		SHI22
239291500	300.3325178451	44.1441255725	11.9143	1.61313	0.015519	7665	4.0578	9588	4.2580	28.28	EB	δ Sct		GAU19
239984394	94.4646257585	32.5045973943	7.1075	5.45998	0.124824	6890	3.3870	6870	3.5534	31.95	EB	δ Sct	Y	
240497891	18.5719675646	48.9904537236	10.8465	2.49478	0.035267	7716		9651	4.1432	153.50	EA	δ Sct		KAH17,LIA17
242149417	210.2075677412	-42.3483150547	8.9878	1.82075	0.047060	7156	3.7214	7371	3.7415	21.52	EB	δ Sct	Y	
243287588	204.0331654514	-45.2380151786	10.4227	2.31007	0.084694	6954	3.8396	7038	3.8576	14.06	EB	δ Sct	Y	
244208023	73.2858034467	-3.4979848940	11.8979	1.82289	0.039235	7647	4.0785	9841	4.2391	33.00	EA	δ Sct		SHI22
244250449	74.3102719895	-3.6012937725	10.2935	1.74608	0.026163	8199	4.0336	9703	4.0288	31.79	EA	δ Sct	Y	
255744818	99.2595648337	-52.0164292068	9.2276	3.04779	0.044587	7858	3.6892				EB	δ Sct	Y	
255921197	307.4419940901	71.4186300528	9.0469	1.77827	0.053386	6465	3.6836	6629	3.7630	13.86	EB	δ Sct	Y	
256640561	327.8973718744	71.8857451308	8.0459	1.72079	0.098803	7891	3.4821				EB	δ Sct		KAH22
258351350	296.5105834547	69.9191670524	7.9352	0.77286	0.019205	8015	4.0584	7757	3.8228	16.27	EB	δ Sct		KAH17,LIA17
262412046	69.2764861541	1.6919883341	10.5627	2.04310	0.057038	7070	3.8530				EA	δ Sct		KAH17,LIA17
262958558	11.4612395273	-78.8213369345	9.6435	3.53606	0.783152	7616	3.9160	9933	4.0202	41.93	EA	γ Dor-δ Sct	Y	
264483228	81.3797073396	2.8833898291	10.0242	1.94997	0.019339	7485	4.1489	9434	4.3881	15.03	EA	δ Sct	Y	
265591866	331.9794049517	-59.8749106526	10.8404	2.28081	0.049442	7381	3.8815	7504	3.7340	25.45	EA	δ Sct		SHI22

Table 1 continued on next page

Table 1 (*continued*)

TIC	R.A.	Decl.	T_{mag}	P_{orb}	P_{dom}	$T_{\text{eff}}^{\text{TESS}}$	$\log g^{\text{TESS}}$	$T_{\text{eff}}^{\text{Gaia}}$	$\log g^{\text{Gaia}}$	L^{Gaia}	Etype	Ptype	New PB	Literature
	(degree)	(degree)	(mag)	(day)	(day)	(K)	(dex)	(K)	(dex)	(L_{\odot})				
266006310	95.3573953535	2.2685045863	6.0571	5.56393	0.050397	7524					EA	δ Sct- γ Dor		SHI22
266032748	14.4979153234	9.6781442865	11.7454	0.81256	0.019889	8048	4.2999	7600	3.8550	9.65	EB	δ Sct	Y	
266735682	29.2078661578	-21.1954116513	10.3677	1.13521	0.022483	7828	4.2704	7932	4.1815	12.85	EA	δ Sct	Y	
268383780	299.0568199609	47.9093449410	11.3625	2.61837	0.043326	8732	4.0829	9719	4.0205	42.05	EA	δ Sct		KAH17,LIA17
268387175	299.0405608283	46.6611494610	10.8433	2.16392	0.096163	6279		7033	3.5500	35.94	EB	δ Sct		GAU19
268718018	18.2608735129	-22.6099862092	11.7837	0.88539	0.018976	7926	4.3542	7996	4.1180	8.90	EB	δ Sct	Y	
270616815	293.6933299764	45.5170399445	11.8466	3.04445	0.036543	7724	3.8304	9230	3.8610	58.79	EB	δ Sct		GAU19
271529113	354.5845210063	64.3340831187	8.9400	2.34009	0.031478	7859	3.9279	7683	3.8063	21.70	EA	δ Sct		KAH17,LIA17
271967202	295.9351347347	43.4781714609	11.6069	3.20715	0.035292	7305	3.8199	7579	3.8196	21.49	EB	δ Sct		GAU19
274348764	300.5163949319	39.7656523630	10.1646	0.83205	0.038466	8166	3.9600	8266	3.9565	23.86	EB	δ Sct	Y	
276457924	228.4707852865	-37.6557765624	10.5355	5.09962	0.073171	7110	3.8320	6983	3.8224	13.15	EA	δ Sct	Y	
277565268	311.1240403010	54.1019402551	9.3321	1.09588	0.102578	8057	3.7197	7329	3.7646	25.78	EB	δ Sct	Y	
280723416	344.4304844987	-78.4081979271	11.4042	0.82504	0.016797	5711		7290	3.4359		EB	δ Sct	Y	
287351976	122.6813197842	-72.5457203008	11.6313	1.92224	0.026258	7436	3.9531	9728	4.2309	35.57	EA	δ Sct		SHI22
289722957	274.1805028867	53.2464959099	11.5104	2.21816	0.043891	7070	4.0390	7620	4.0253	11.52	EA	δ Sct	Y	
291329564	260.9457036626	-55.0621651642	9.9161	2.38018	0.045544	7016	3.6934	7566	3.7346	26.25	EA	δ Sct	Y	
298541138	261.74717159963	24.6965572269	11.3358	0.74908	0.027565	7605	4.1217	7898	4.0210	12.25	EB	δ Sct	Y	
298734307	278.6095797774	57.8018197869	7.2099	0.94445	0.032181	8014	3.9479	7841	3.9090	20.62	EB	δ Sct		SHI22
300012172	106.8271061047	-66.0631983263	10.3883	1.46120	0.055820	7495	3.8066	7880	3.8483	22.95	EB	δ Sct	Y	
300654002	114.4168954280	-69.5423284166	10.2724	2.75804	0.051581	7291	3.5938	9764	3.9373	73.36	EA	δ Sct	Y	
301063488	298.3512269214	20.3274543770	7.0814	7.32720	0.037265	7725		7115	3.5437	47.47	EA	δ Sct	Y	
301405723	52.9760428992	-1.6392895686	11.1728	0.94262	0.023323	8089	4.1211	7785	3.8965	10.77	EA	δ Sct		SHI22
301407485	53.1046925995	-3.3133600126	8.1191	2.66407	0.016941	8053	4.0317	10463	4.1744	45.30	EB	δ Sct		KAH17,LIA17
302373103	133.7731244302	-67.5349557181	11.5238	0.90277	0.017960	7450	4.2053	8152	4.0477	11.71	EB	δ Sct	Y	
303733089	168.7201608338	-34.6349217958	10.5561	1.26288	0.023506	7549	4.0584	8121	3.8949	18.62	EB	δ Sct	Y	
304030311	141.2246377398	-71.4721102773	10.4943	6.29391	0.730948	7403	4.1696	7448	4.0909	8.45	EA	γ Dor- δ Sct	Y	
307990280	129.2359834347	-67.7447505240	9.4314	2.31598	0.022152	7313	4.0282	10812	4.3375	37.67	EW	δ Sct	Y	
309658221	79.2537140265	-61.5145883481	9.8567	7.59543	0.100535	6813					EA	δ Sct		LEE19
312621168	210.810798102	-48.7917478218	9.8539	0.93267	0.013224	8520	4.3786	10074	4.3725	21.14	EB	δ Sct	Y	
312865025	126.4657786341	77.2185691500	9.4026	2.73500	0.074584	7103	3.5472	6928	3.6346	25.82	EA	δ Sct	Y	
314864553	53.1681854402	-75.8888137155	11.9207	1.05562	0.016886	7438	4.0832	8378	4.0022	15.66	EB	δ Sct	Y	
315777423	321.0968862035	56.3615613539	8.2842	4.93133	0.172826	10082		17069	3.4563		EA	Maia	Y	
316633550	263.7627392634	24.5630259173	11.5439	4.64296	0.133189	6752	3.3601	6869	3.4340	40.47	EA	γ Dor- δ Sct	Y	
318088293	-30.0009082223	-79.9952929682	10.8986	0.69738	0.037317	7684	4.0192	8056	4.0373	15.59	EB	δ Sct	Y	
318217844	142.8526877358	49.4678928998	9.9964	1.22227	0.020602	7828	4.0446	7490	3.8964	16.66	EB	δ Sct	Y	
323292655	130.8008244196	-79.0701017167	5.8258	1.66983	0.086018	7444	3.6538	7417	3.6871	28.61	EA	δ Sct		KAH17,LIA17
326356701	325.5969830408	-21.7626556960	8.3387	1.11216	0.019724	4674		5604	1.5484	203.00	EB	RGB	Y	
330658205	136.4043732507	12.5897309304	10.8392	3.60217	0.234463	7062	3.9792				EA	γ Dor- δ Sct		SHI22
332541024	270.4920720868	30.7879611343	10.8162	1.17635	0.017887	7221		7586	3.8263	21.90	EB	δ Sct	Y	
335265326	332.1899776964	61.0224185676	7.2771	3.80835	0.197503			20267	3.5716		EB	β Cephei	Y	
337094559	335.6357207166	63.5862767539	9.3502	1.78066	0.110446	7424	3.7162				EB	δ Sct		KAH22
337886863	337.3230520488	65.1133243340	7.5536	5.69258	0.342182	11686					EA	γ Dor- δ Sct	Y	
338159479	338.0648451224	64.9778629452	11.2918	1.41434	0.036928						EB	δ Sct		KAH22
339397374	295.7759845138	-60.77787350305	10.3223	1.18207	0.032584	7367	3.9591	7428	3.8894	16.74	EB	δ Sct	Y	
339570153	253.6228783296	-41.6541530122	7.9038	6.34726	0.101518						EA	δ Sct- γ Dor	Y	
347361290	25.9662025404	10.9502834784	10.4749	1.01553	0.015090	8082	4.2923	9418	4.3478	18.35	EW	δ Sct	Y	
350443417	85.3046330415	-57.4411661124	8.9808	1.21673	0.043892	7636	4.3227	7406	4.1776	6.50	EA	δ Sct	Y	
351473399	308.6705424632	-64.1744980436	11.5763	0.86760	0.031680	7745	4.2283	7929	4.0870	11.05	EB	δ Sct	Y	

Table 1 continued on next page

Table 1 (*continued*)

TIC	R.A.	Decl.	T_{mag}	P_{orb}	P_{dom}	$T_{\text{TESS}}^{\text{TESS}}$	$\log g^{\text{TESS}}$	$T_{\text{eff}}^{\text{Gaia}}$	$\log g^{\text{Gaia}}$	L^{Gaia}	Etype	Ptype	New PB	Literature
	(degree)	(degree)	(mag)	(day)	(day)	(K)	(dex)	(K)	(dex)	(L_{\odot})				
351667692	274.9476039940	42.1772730478	11.3446	2.07291	0.017925	7939	4.2302	9375	4.2222	24.11	EB	δ Sct	Y	
353854078	271.1411728552	58.3984180327	9.8329	5.17034	0.043971	6595	3.4075	6833	3.4668	31.84	EB	δ Sct		KAH17,LIA17
354922610	39.3812971343	71.3045204584	9.8471	1.36696	0.058284	7056	4.0692	7478	3.9409	10.66	EA	δ Sct		LIA17,HON17,MIS22
354926863	39.4423509141	67.8555200171	10.5010	1.43602	0.046164	7388	4.0716				EA	δ Sct		KAH22
356194871	266.6269381314	53.1994297859	10.1756	2.71044	0.040396	7782	3.7197	9638	3.9723	66.61	EB	δ Sct		KAH17,LIA12,LIA17
356240274	267.7113679711	50.0471947344	11.7539	2.34757	0.041004	7394	3.9104	10092	4.2015	45.95	EA	δ Sct	Y	
358613523	175.1028937630	80.2359806993	10.0086	1.32833	0.024065	7271	4.2780	7383	4.1111	6.60	EA	δ Sct		KAH22
363852956	200.6195886680	-45.8915478481	11.8138	0.74065	0.060809	7349	4.0527	7395	4.0152	10.40	EB	δ Sct	Y	
365956683	276.0468304400	-63.9486439979	10.8967	5.73042	0.075607	6455	3.4342	6859	3.5272	30.38	EB	δ Sct		KAH17,LIA17
372759279	175.0060004748	75.1559630489	10.8419	1.23833	0.023884	7653	3.9519	7896	3.9695	17.76	EA	δ Sct		ZXB14,KAH17,LIA17,LEE18,CXH21
373029274	67.0687637360	7.8441154302	11.4338	1.07661	0.015459	7624	4.2509				EB	δ Sct	Y	
376486632	180.5928829261	-58.2272780000	11.1646	2.60213	0.071493	7422					EA	δ Sct	Y	
378042585	352.0751940586	63.3908139172	7.9317	3.25952	0.143783	6965	3.2255	6734	3.3628	48.81	EB	δ Sct	Y	
381011161	303.7036406499	34.7395150992	11.9215	1.31250	0.030774	7189	3.8429	7714	3.9531	18.84	EA	δ Sct		KAH17,LIA17
381948745	76.3683365792	-56.3028684329	9.8456	3.19170	0.050038	7085	3.5597				EB	δ Sct	Y	
385916950	111.3294120580	-16.4590270867	8.8819	1.56251	0.040473	6907	3.7274	6782	3.8360	14.58	EA	δ Sct	Y	
388244501	126.3858149855	-84.3634848912	8.5565	2.11893	0.048901	7854	3.6355				EB	δ Sct	Y	
391902612	106.5680497401	-76.8392707703	11.8625	4.55234	0.086437	6586	3.5690				EA	δ Sct		SHI22
393636596	239.5767093170	17.2694459987	10.6639	0.87934	0.045744	7568	4.2485	7666	4.2340	8.11	EA	δ Sct		KAH17,LIA17
393894013	198.3890021745	47.7977363777	9.1556	0.81588	0.035586	7866	4.1933	7684	4.0579	10.32	EB	δ Sct		KAH22
394126943	2.7039836475	-68.5472164131	9.6443	1.84588	0.018387	7610	4.1009	7579	3.7353	13.02	EB	δ Sct	Y	
396134795	357.0983261865	36.3111877125	9.5636	2.58883	0.070438	6946	3.8002	7101	3.7057	19.29	EA	γ Dor- δ Sct		KAH22
396201681	359.5249573147	67.6031600612	9.6904	7.03806	0.478076	7767		6166	2.8834	15.15	EA	γ Dor- δ Sct		KAH22
397048159	73.3951521526	5.6126918125	10.1721	1.60553	0.063577	7222	3.9114	7442	3.8681	14.89	EB	δ Sct	Y	
400105121	97.0078813768	77.8260806041	11.0266	1.44492	0.016725	8272	4.2594	9626	4.2452	19.70	EA	δ Sct	Y	
401701828	317.5806712791	-82.4240932579	9.7728	1.16750	0.061965	7428	3.8932	7636	3.8679	18.53	EB	δ Sct	Y	
401869914	51.7682423111	-45.8823819291	10.7328	2.60793	0.026263	7529	3.8499	10188	4.0525	49.59	EB	δ Sct		LIA17,STR18
405605748	202.0407789137	-32.7236401436	11.6890	0.76493	0.020972	8129	4.4030	8421	4.2182	11.61	EB	δ Sct	Y	
406421379	308.2928216243	24.8653789324	11.3710	2.02498	0.014857	8256	4.2560	10037	4.2930	23.44	EA	δ Sct	Y	
406798603	225.6920812427	37.9101125343	10.1329	0.90639	0.019095	7987	4.2135	8432	4.0935	14.56	EB	δ Sct		KAH17,LIA17,ZXB15,DG15
406947878	290.2984105960	47.9785983500	9.3918	1.23147	0.035547	8068	3.8697	7699	3.8499	23.36	EB	δ Sct		SOU11,LEH13,KAH17,LIA17,MIS21
412638697	329.6423921779	60.9504944856	11.2956	0.98590	0.022247	8344		7477	3.9740	10.80	EA	δ Sct	Y	
413395842	176.8449515428	-23.0417568761	8.8507	0.89768	0.027784	7351	4.1546	7501	4.0417	9.42	EB	δ Sct	Y	
428003183	349.2207982107	44.4884480054	10.7131	0.74260	0.041583	7345	4.0477				EB	δ Sct		KAH22
431527184	357.3813660223	53.1346228524	10.9091	0.99850	0.028854	7591	3.9536	8154	3.9327	26.23	EB	δ Sct		KAH17,LIA17,KIM10
431555426	357.6198613129	50.6781736771	9.6212	1.77898	0.427180	7213		7235	3.8092	13.26	EB	γ Dor- δ Sct	Y	
440003271	2.5133397165	46.3903078945	7.6835	2.63945	0.064030	8334	4.1623	9839	4.2715	27.47	EA	δ Sct		KAH22
440459327	90.5398739179	45.6903870005	8.1075	0.30233	0.036479	8394	4.0445	7935	3.8429	18.54	EW	δ Sct	Y	
441006548	210.0474875044	-32.9364279291	10.0813	1.16720	0.016255	8386	4.1924	9792	4.3133	25.44	EB	δ Sct	Y	
441406061	310.8020240174	-32.2931748296	9.4763	3.01802	0.082078	6916		7019	3.4860	53.57	EB	δ Sct		SHI22
441598163	115.2958520519	76.0739139894	10.2744	3.30592	0.066463	7396	3.5416	7694	3.6493	40.72	EA	δ Sct		KAH17,LIA17,BRO74,KIM02,ROD10
447733367	255.1928831684	-64.0144302907	11.8477	2.63111	0.108402	6871	3.8814	6936	3.9058	11.19	EA	δ Sct		SHI22
449486448	160.6955417028	-72.9866185260	10.4418	3.51152	0.630629	7019	3.7353	7280	3.7790	18.06	EA	γ Dor- δ Sct	Y	
450089997	72.1406335462	8.5933140862	9.2468	2.46167	0.132171	6802	3.4813				EB	δ Sct	Y	
452734608	195.4726275319	-19.7746554648	7.7217	1.99393	0.058240	6111		7032	3.7233	13.31	EB	δ Sct		BAR20
456609929	282.3517441910	-59.4205912111	8.7194	4.56750	0.079275	7643	4.0974	7763	3.8448	21.16	EA	δ Sct	Y	
456905229	26.2229199415	19.8567993659	8.0865	1.69267	0.065935	7041		6926	3.9000	11.26	EA	δ Sct		KAH22
459789367	144.5279975768	56.0186914005	9.9765	0.68737	0.019501	7664	3.9623	7593	3.8172	14.92	EB	δ Sct		KAH17,LIA17

Table 1 continued on next page

Table 1 (*continued*)

TIC	R.A.	Decl.	T_{mag}	P_{orb}	P_{dom}	$T_{\text{eff}}^{\text{TESS}}$	$\log g^{\text{TESS}}$	$T_{\text{eff}}^{\text{Gaia}}$	$\log g^{\text{Gaia}}$	L^{Gaia}	Etype	Ptype	New PB	Literature
	(degree)	(degree)	(mag)	(day)	(day)	(K)	(dex)	(K)	(dex)	(L_{\odot})				
468670361	19.0875792722	76.8027156233	8.5340	1.15206	0.027899	7824	3.6188	7201	3.5652	30.14	EB	δ Sct	Y	
469979014	342.2748751557	-69.5671849817	12.2478	1.16259	0.042609	7679	3.8584	9431	4.2337	46.63	EB	δ Sct	Y	
836353664	132.1580534312	-13.4350738321	11.1811	1.12319	0.058210	7526		7355	4.0598	8.49	EB	δ Sct	Y	
974128107	183.7920872924	-65.1783336508	10.0375	3.49309	0.045772					EA	δ Sct	Y		

NOTE—Targe ID are sorted by increasing TIC number in the first column. The second and third columns present the equatorial coordinates in unit of degree. The fourth, seventh, and eighth columns are the TESS magnitudes, the effective temperature, and the surface gravity from the TIC input catalog (Stassun et al. 2019). The fifth and sixth columns are the orbital period and the dominant pulsation period. The ninth, tenth, and eleventh columns are the effective temperature, the surface gravity, and the luminosity from the Gaia DR3 (Gaia Collaboration 2022). "Ttype" column shows the type of binary system. "Ptype" column marks the type of pulsations. "New PB" denotes whether pulsations of the target are new detected. The references in the last column are provided below.

References— BAR20: Barceló Forteza et al 2020, BOW19: Bowman et al. 2019, BRO74: Broglia & Marin 1974, CXH21: Chen et al. 2021, CUI20: Cui et al. 2020, DG15: Doğruel & Gürol 2015, GAU13: Gaulme et al. 2013, GAU19: Gaulme & Guzik 2019, HAS21: Hasanzadeh et al. 2021, HOL14: Holdsworth et al. 2014, HON17: Hong et al. 2017, KAH17: Kahraman Aliçavuş et al. 2017, KAH22: Kahraman Aliçavuş et al. 2022, KIM02: Kim et al. 2002, KIM10: Kim et al. 2010, LEE18: Lee et al. 2018, LEE19: Lee et al. 2019, LEH13: Lehmann et al. 2013, LIA12: Liakos et al. 2012, LIA17: Liakos & Niarchos 2017, LIA20: Liakos 2020, MIS21: Miszuda et al. 2021, MIS22: Miszuda et al. 2022, MKR18: Mkrtchian et al. 2018, RAP21: Rappaport et al. 2021, ROD10: Rodríguez et al. 2010, SHI22: Shi et al 2022, SOU11: Southworth et al. 2011, SOU21: Southworth et al. 2021, STR18: Streamer et al. 2018, WK20: Wang et al. 2020, ZXB14: Zhang et al. 2014, ZXB15: Zhang et al. 2015

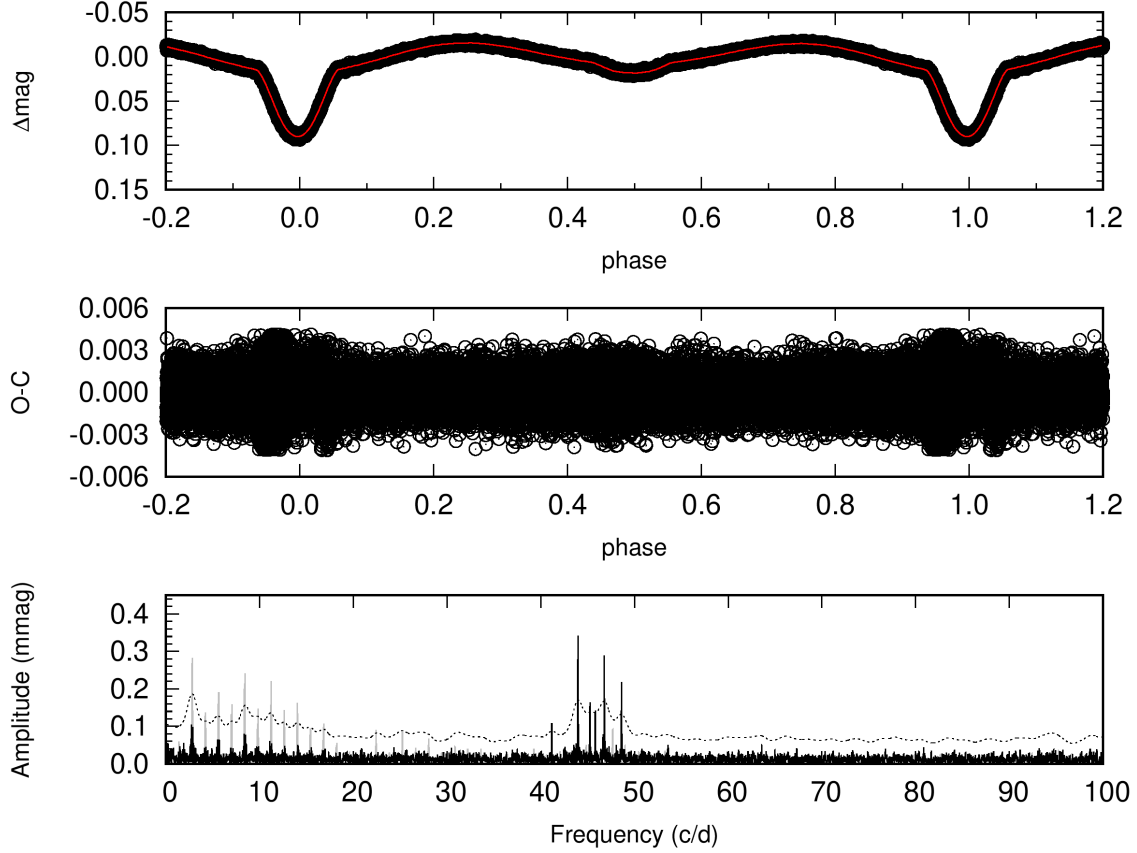


Figure 1. Light curve, O-C residuals, and amplitude spectrum of TIC 125498216. The light curve is displayed with black circles in the top panel, the O-C residuals is presented in the middle panel, and the amplitude spectra is depicted in the bottom panel. The red line in the top panel denotes the synthesis mean curve. The peaks marked in gray are possible orbital-harmonics. The dashed line marks the positions of $S/N = 5$.

APPENDIX

A. SUPPLEMENTARY FIGURES OF AMPLITUDE SPECTRA FOR THE 242 TARGETS.

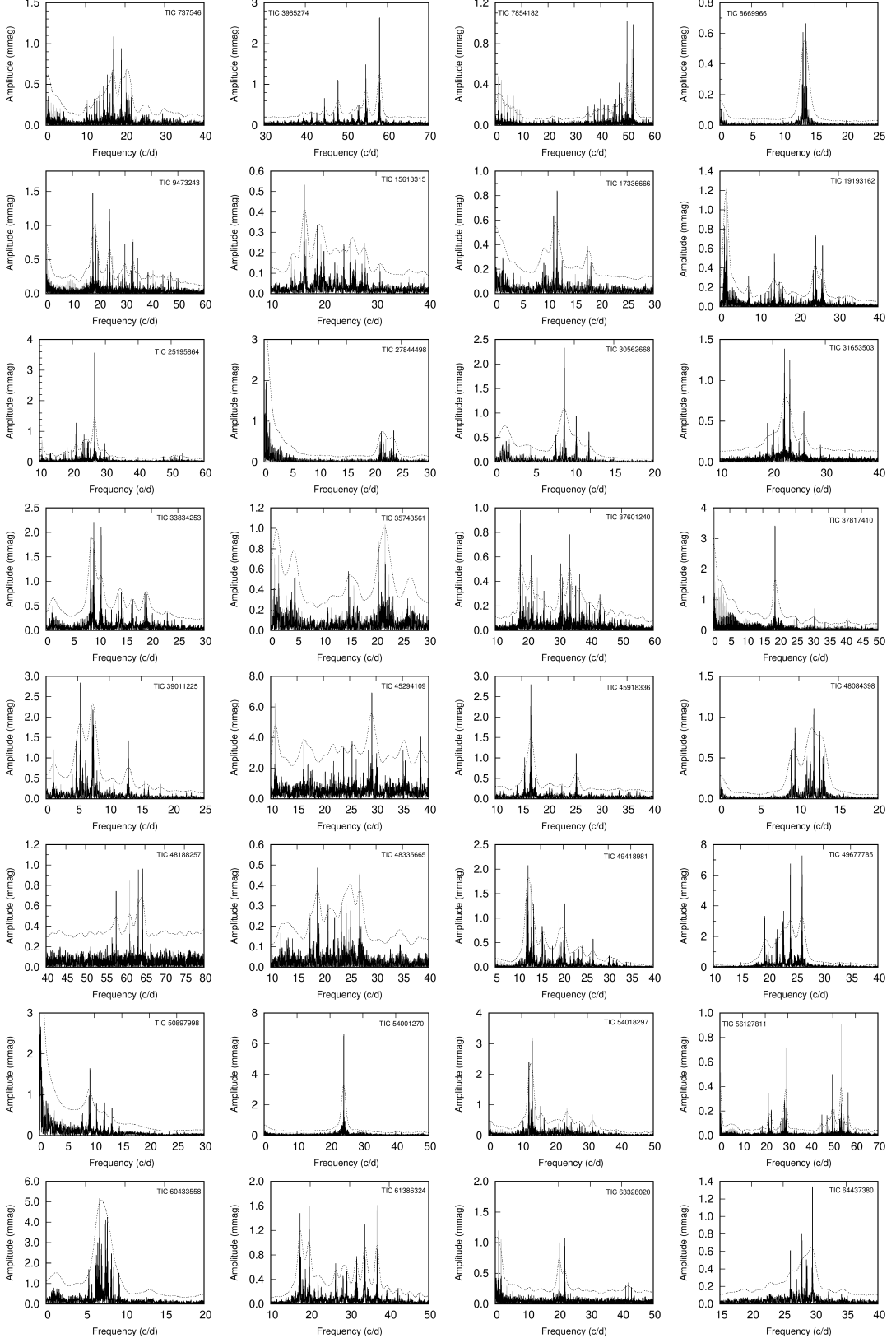


Figure 2. Amplitude spectra of the pulsating components in eclipsing binaries. The dashed lines mark the positions of S/N = 5. All the component figures are available in the Appendix.

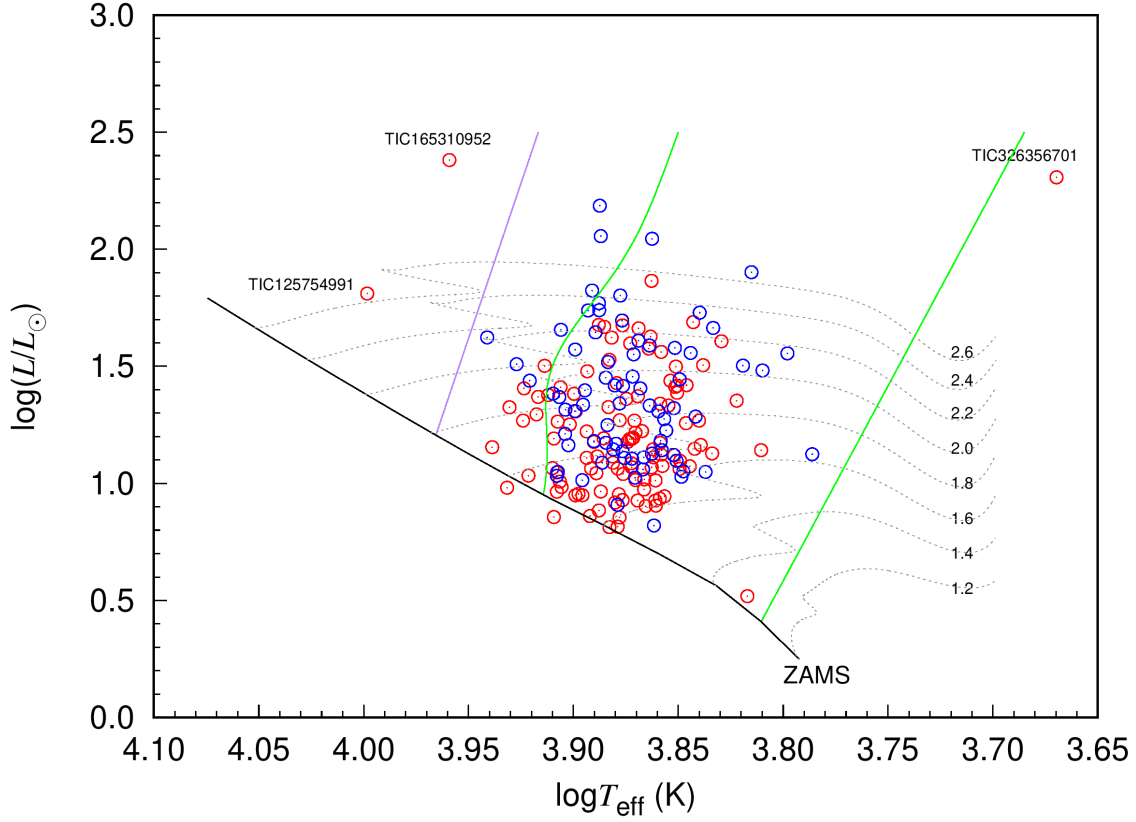


Figure 3. The distribution of the targets in the Hertzsprung-Russell diagram. Newly discovered and old targets are marked with red and blue circles, respectively. The ZAMS line and the evolutionary tracks of eight different initial stellar mass with $Z = 0.015$ are computed with the one-dimensional stellar evolution code Modules for Experiments in Stellar Astrophysics (MESA, Paxton et al. 2011, 2013, 2015, 2018) using the same input physics with Chen et al. (2021). The green lines represent the instability strip derived by Xiong et al. (2016) and the purple line is the theoretical blue edge of the δ Scuti instability strip derived by Li & Stix (1994). Luminosities L are taken from Gaia DR3, while the values of T_{eff} of the stars are taken from the TESS input catalog.

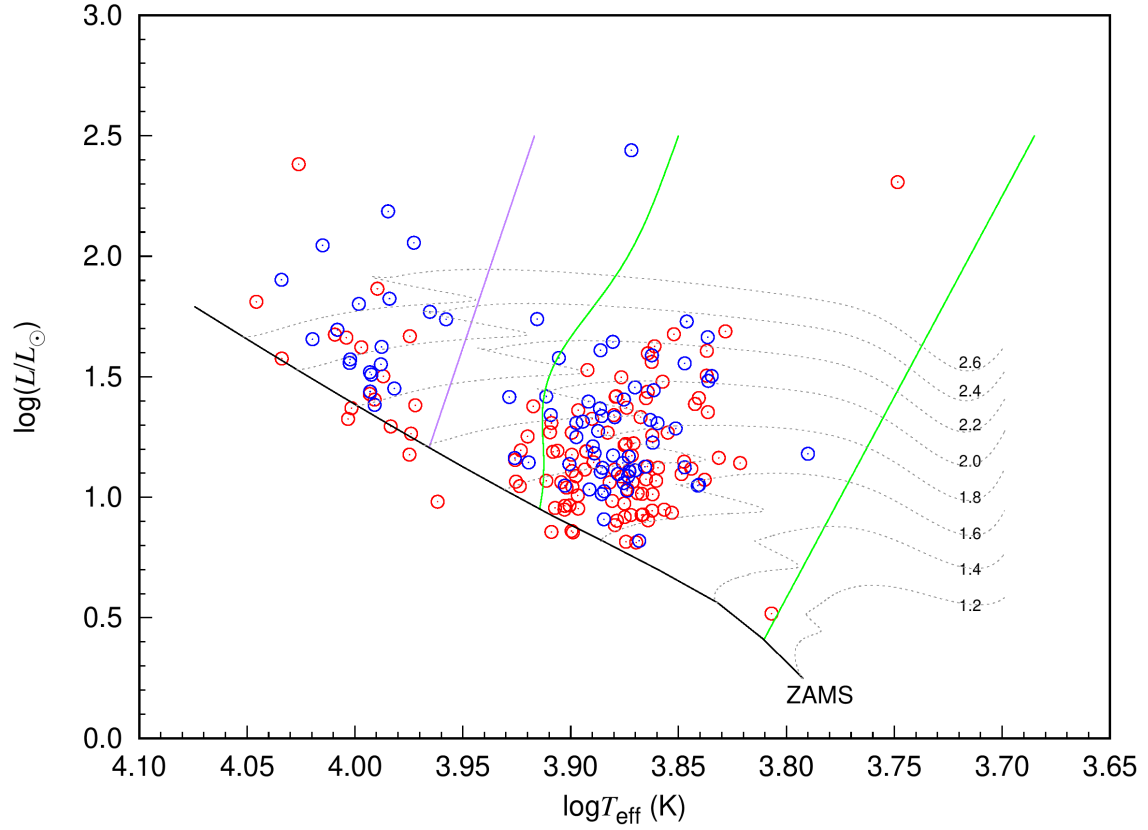


Figure 4. The same as in Figure 3, but the values of effective temperature T_{eff} of the stars are taken from the Gaia DR3.

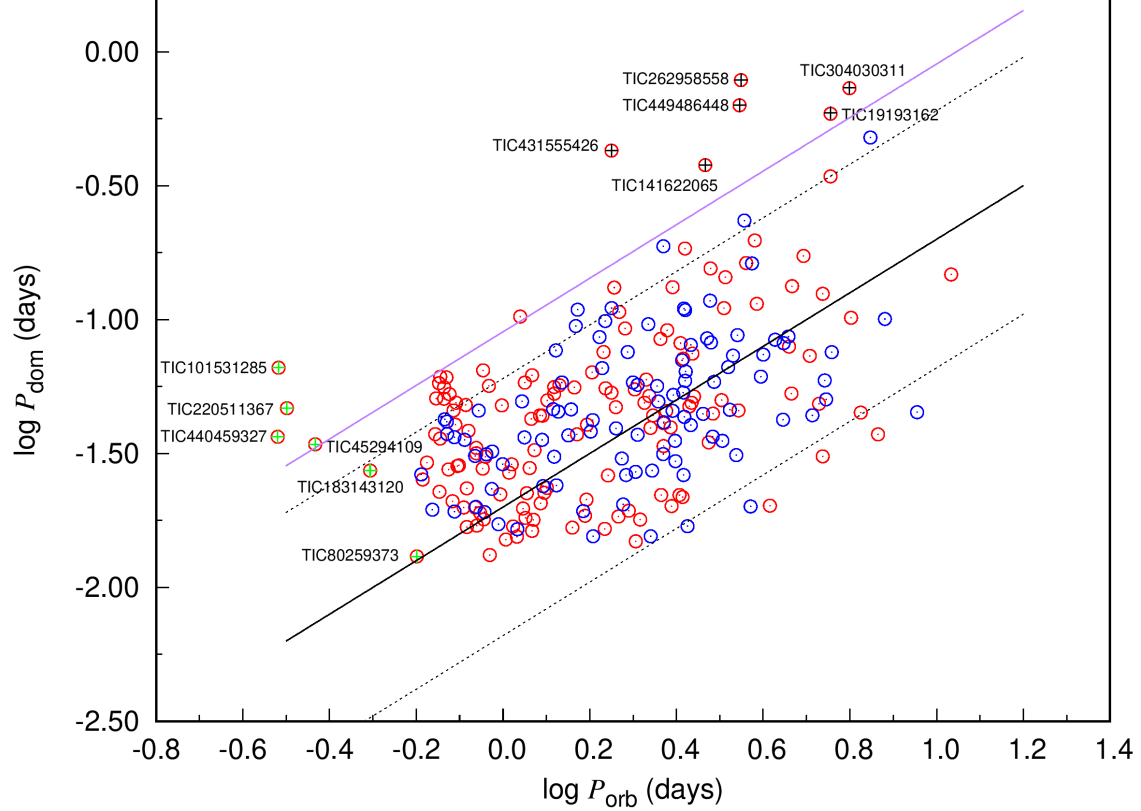


Figure 5. Distribution of the pulsating stars in eclipsing binaries in the $P_{\text{dom}}-P_{\text{orb}}$ diagram. Newly discovered and old targets are marked with red and blue circles, respectively. The solid line in black is the theoretical relation by Zhang et al. (2013), and the two dashed lines correspond to its 3σ uncertainties. The purple line denotes the upper limit of the $P_{\text{dom}}/P_{\text{orb}}$ ratio derived by Zhang et al. (2013) for the δ Scuti stars in eclipsing binaries. The systems marked with green and black cross symbols correspond to targets in Figure 6 and 7, respectively.

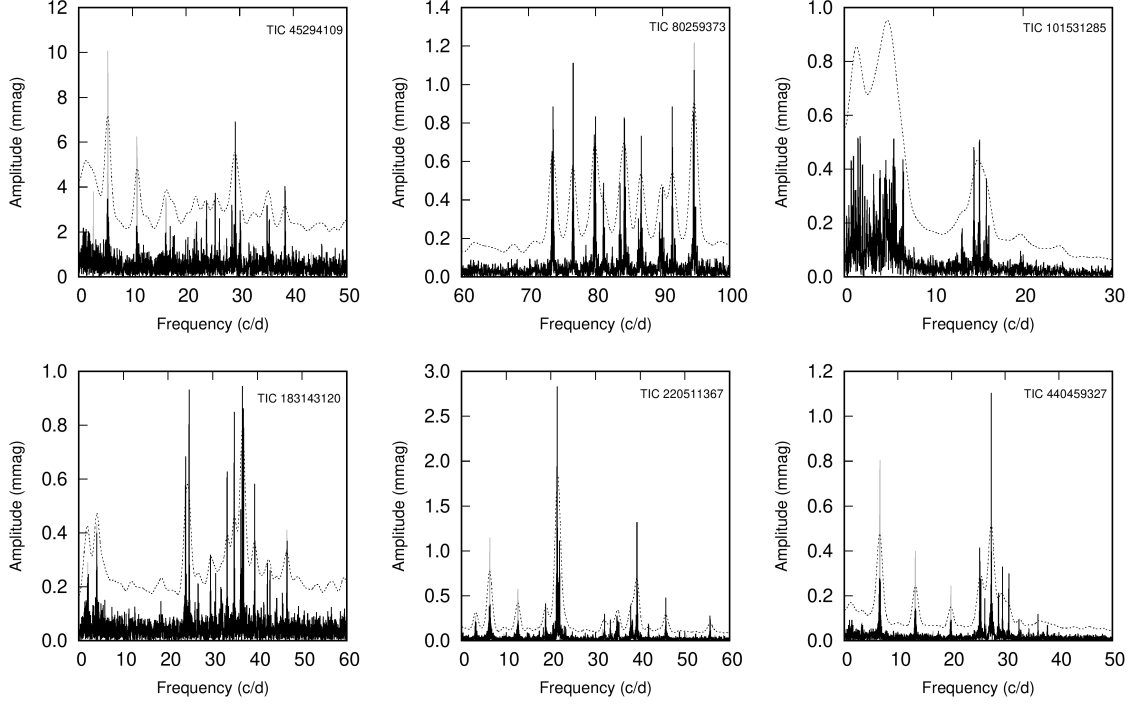


Figure 6. Fourier amplitude spectra for the pulsating components in eclipsing binaries with $P_{\text{orb}} < 0.65$ days. The dashed lines mark the positions of $S/N = 5$.

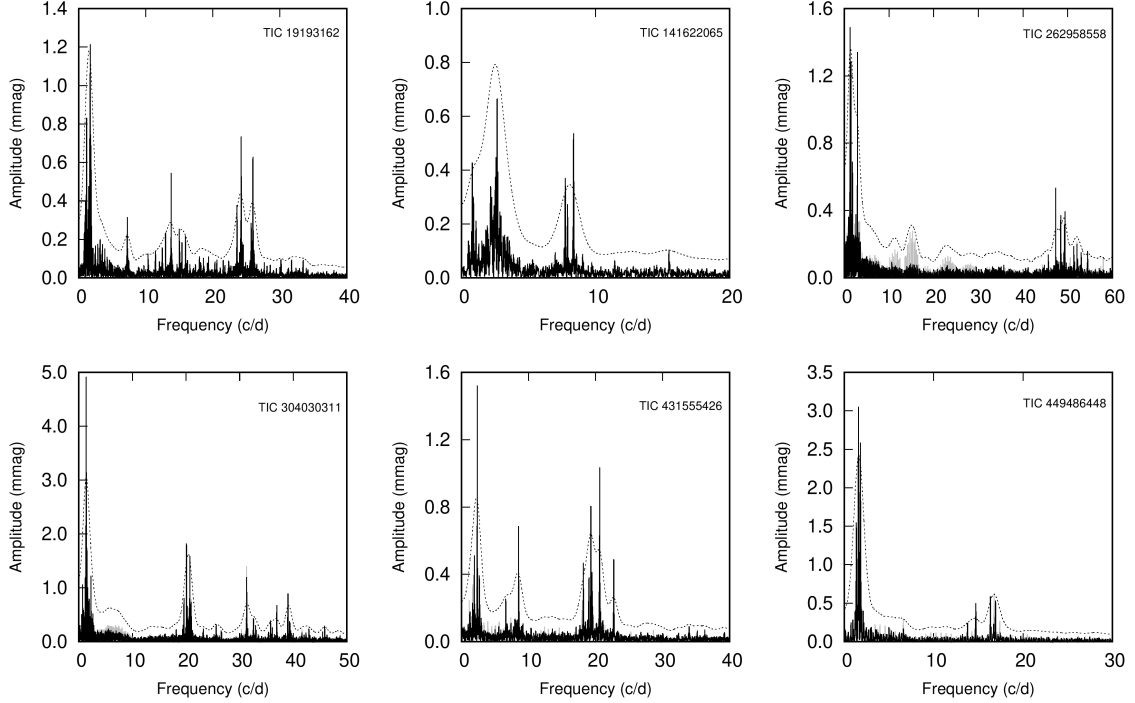


Figure 7. Fourier amplitude spectra of objects TIC 19193162, TIC 141622065, TIC 262958558, TIC 304030311, TIC 431555426, and TIC 449486448, respectively. The dashed lines mark the positions of $S/N = 5$.

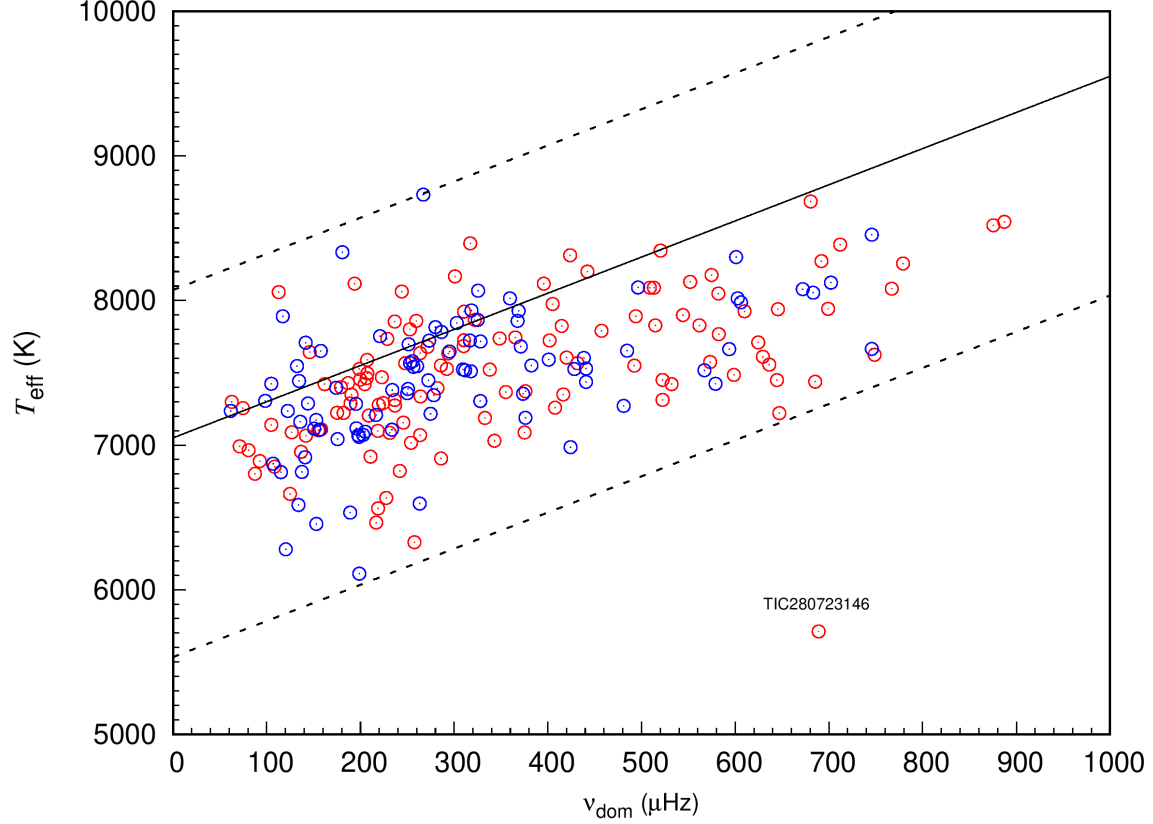


Figure 8. Distribution of the δ Scuti-type pulsating stars in eclipsing binaries within the $T_{\text{eff}}-\nu_{\text{dom}}$ relation. Newly discovered and old targets are marked with red and blue circles, respectively. The black solid line marks the theoretical relation derived by Barceló Forteza et al.(2020), and the dashed lines denote the limits of their predicted dispersion due to the gravity-darkening effect.

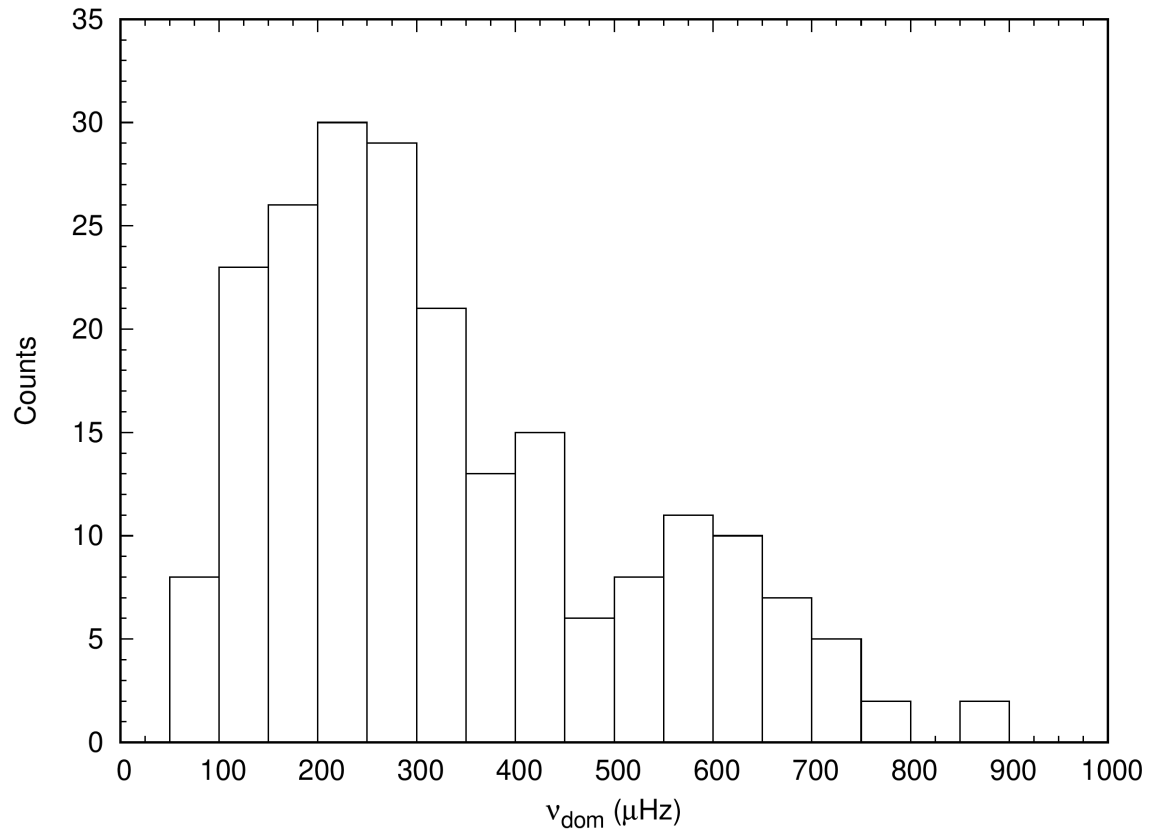
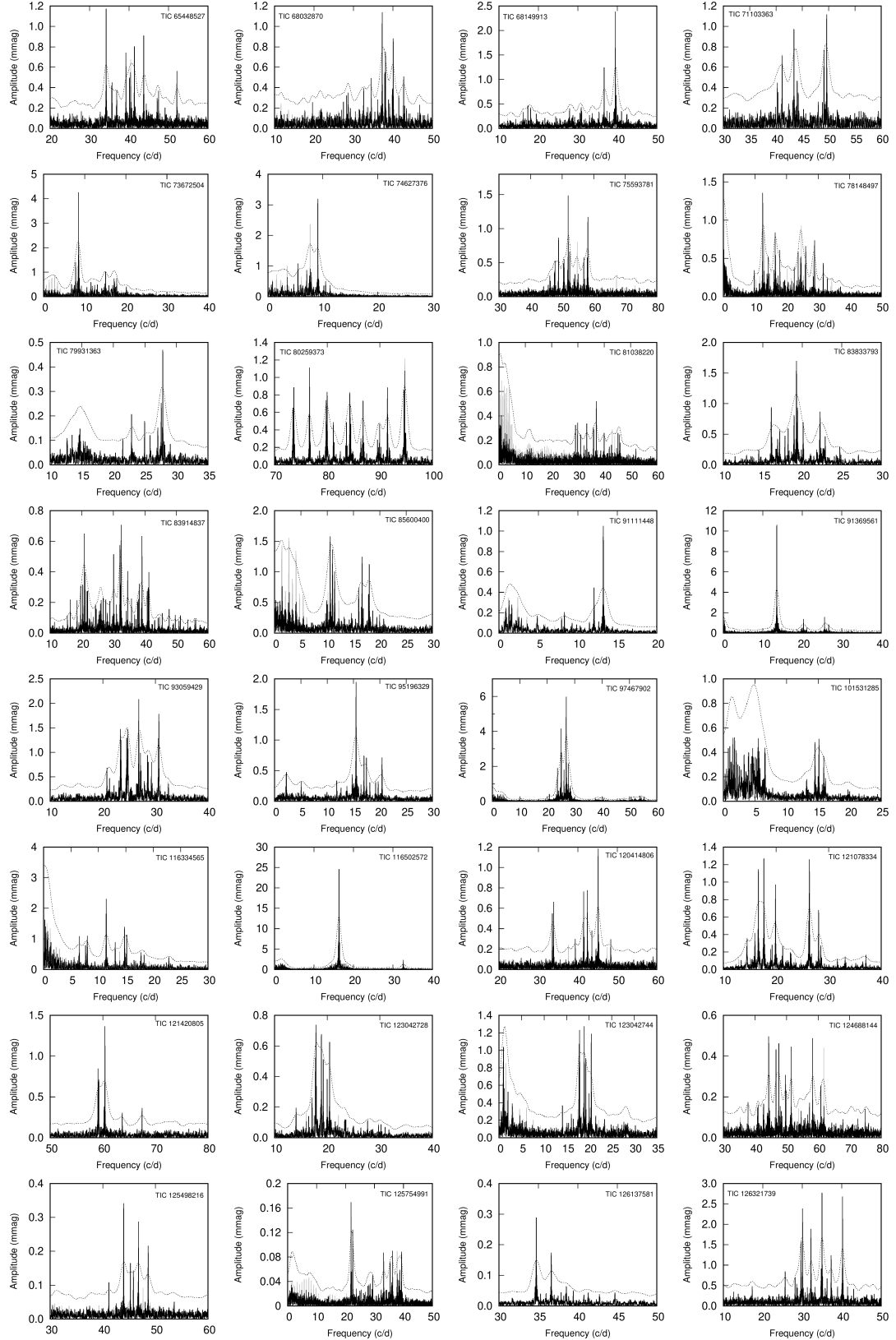
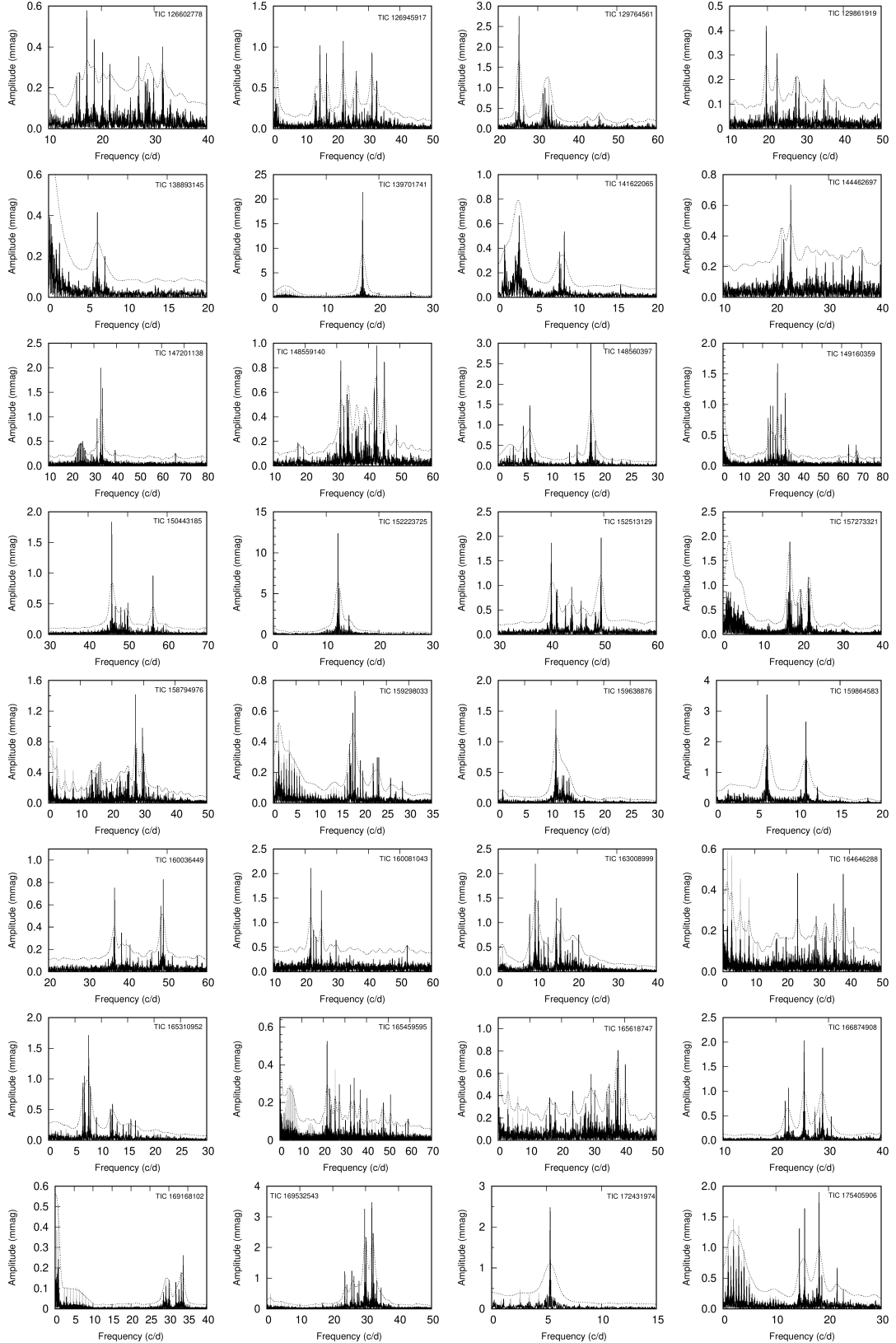


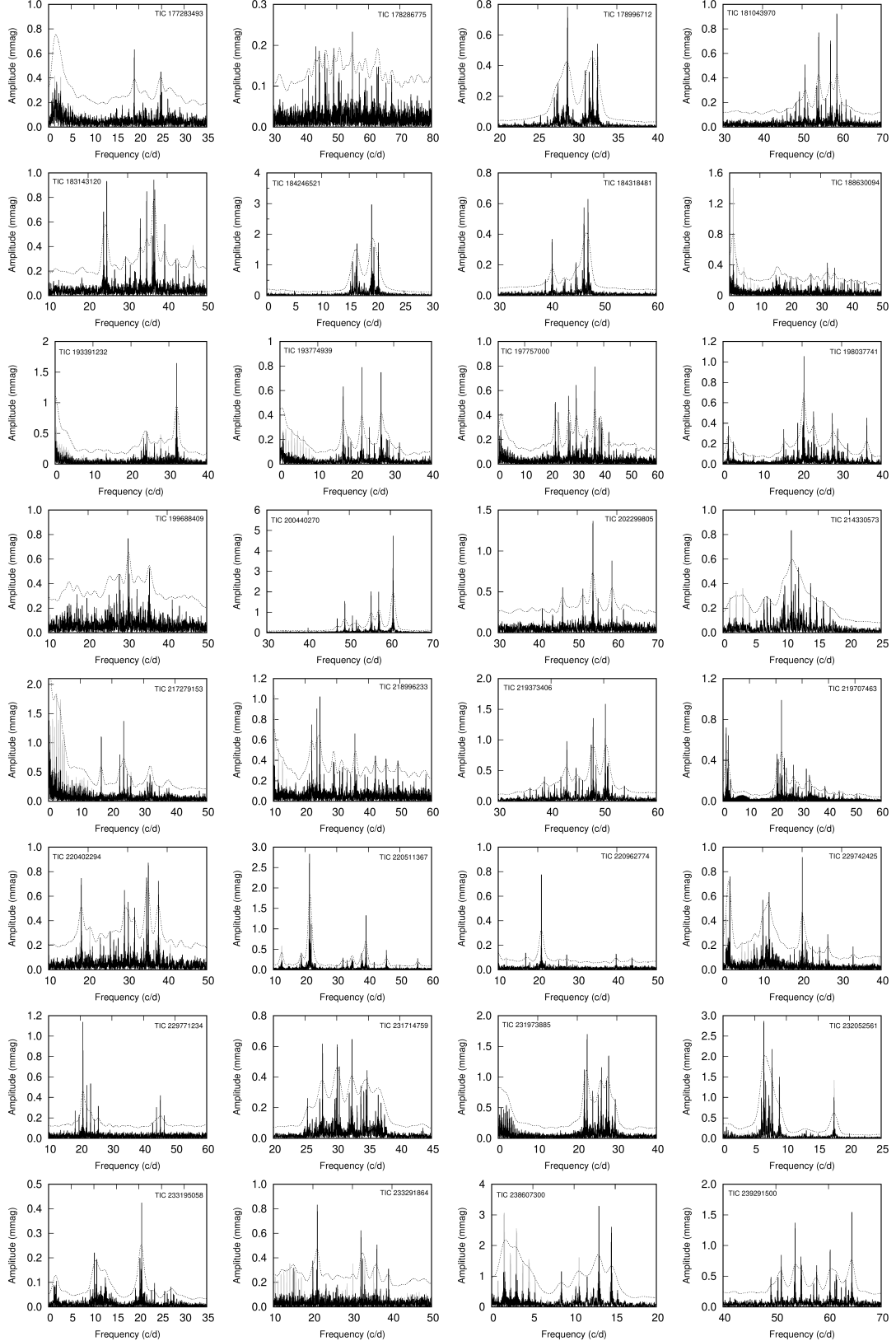
Figure 9. Distribution of the dominant pulsation frequencies of δ Scuti pulsators in eclipsing binaries.



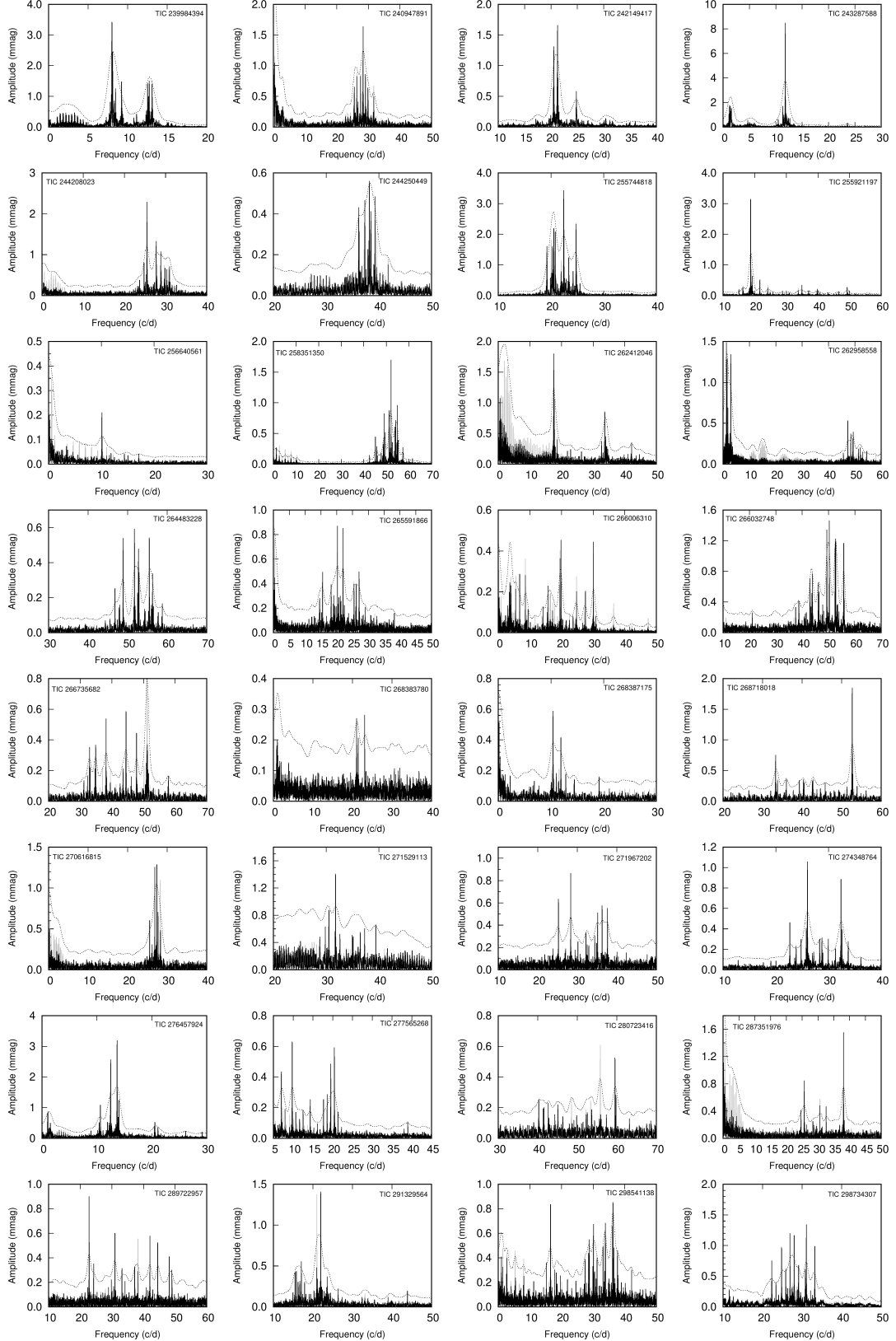
Supplementary Figure 1. Continued to Figure 2 for different targets.



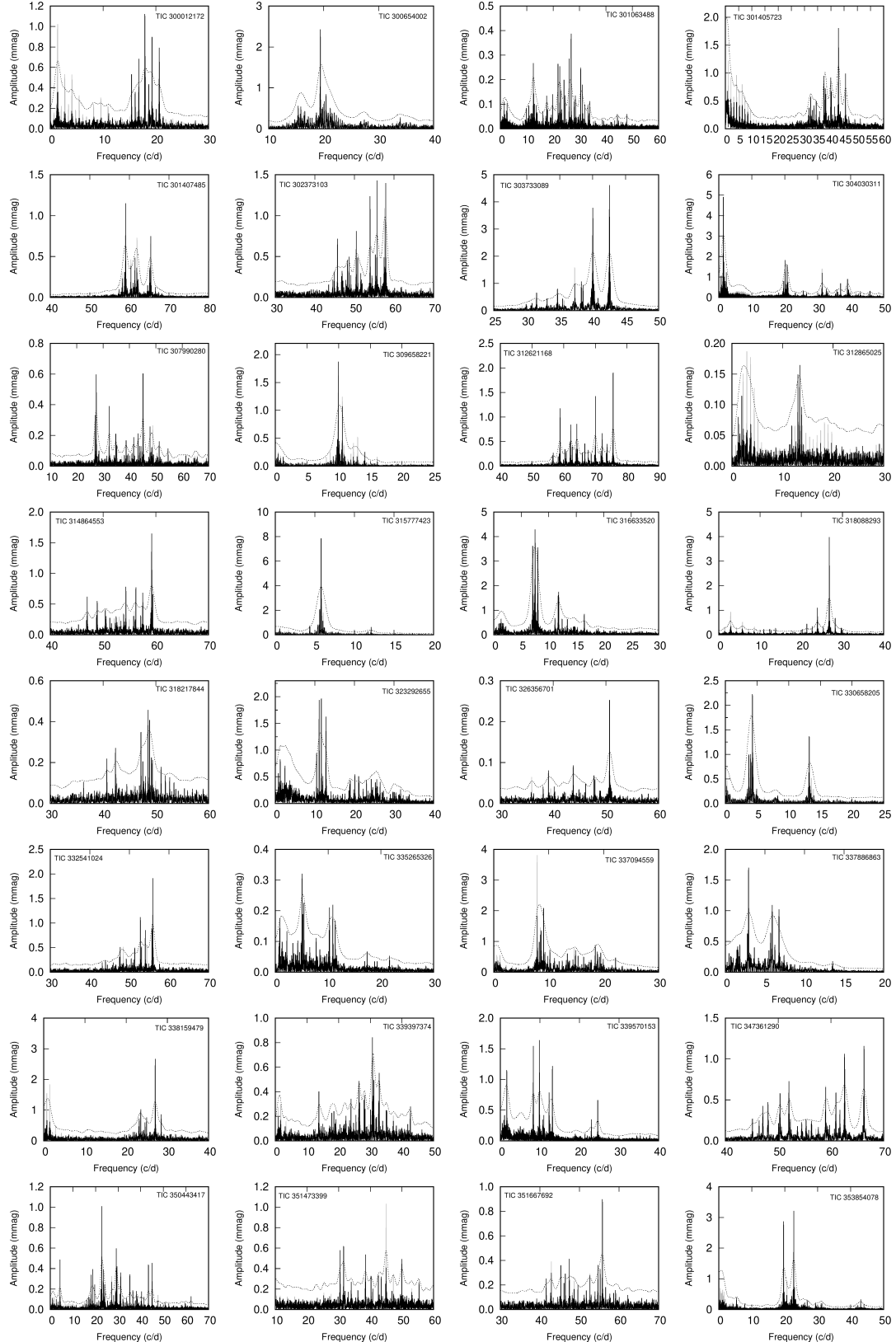
Supplementary Figure 1. (continued)



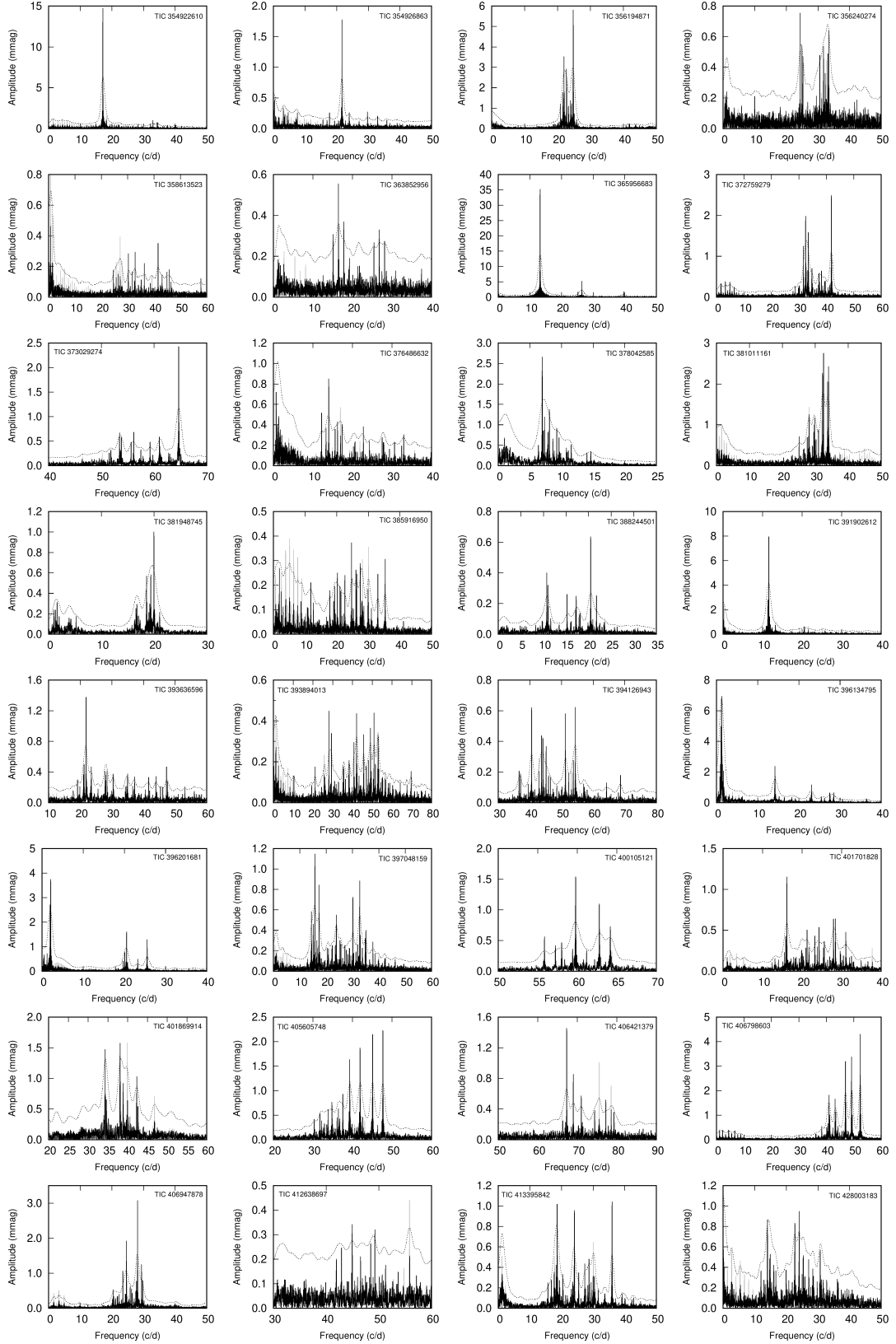
Supplementary Figure 1. (continued)



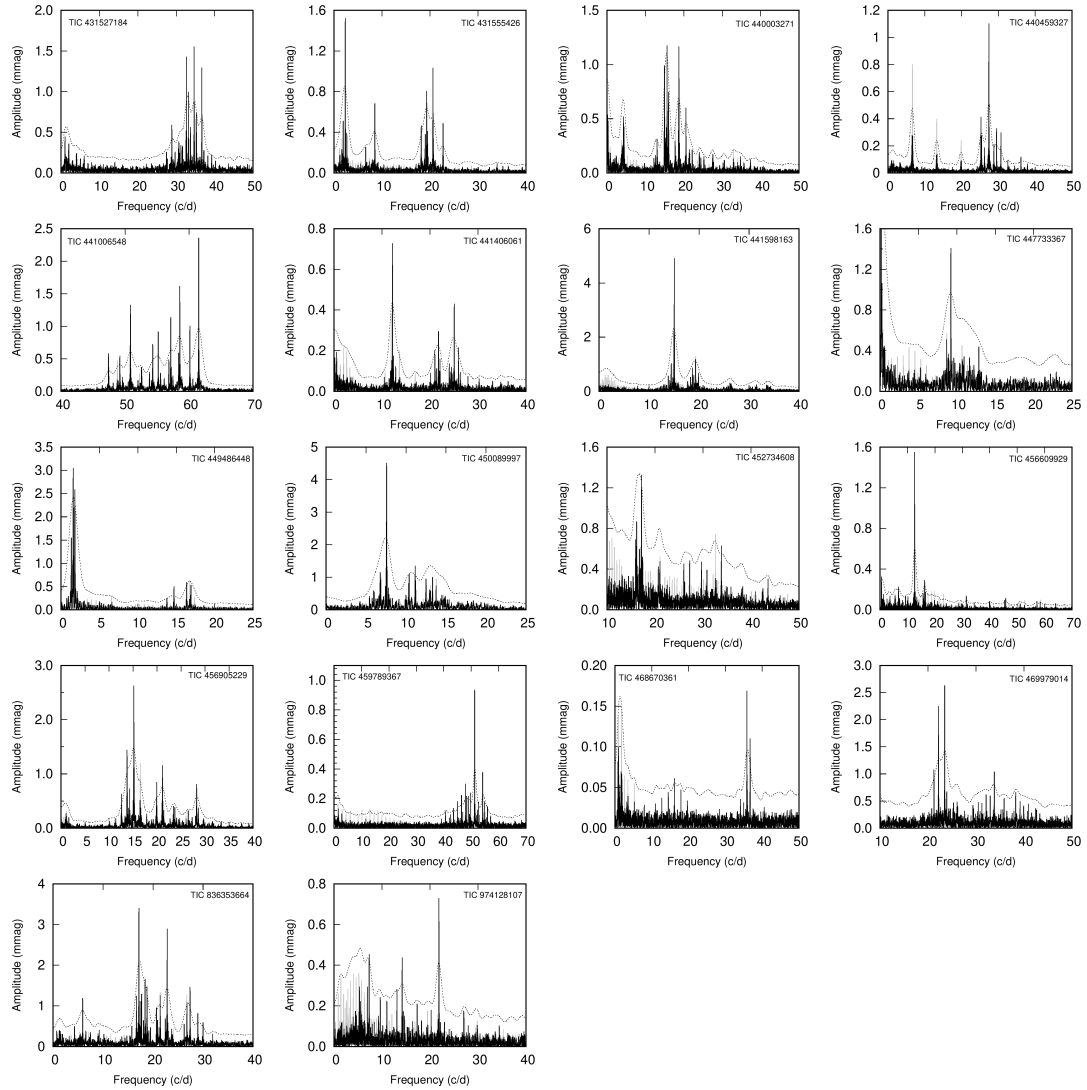
Supplementary Figure 1. (continued)



Supplementary Figure 1. (continued)



Supplementary Figure 1. (continued)



Supplementary Figure 1. (continued)